BNWL-1053
UC-80

3-
5-69

[redacted]

REACTOR PHYSICS QUARTERLY REPORT

JANUARY, FEBRUARY, MARCH 1969

May 1969

[redacted]

AEC RESEARCH & DEVELOPMENT REPORT

ROUTE TO	P.R. NO.	LOCATION	FILES ROUTE DATE

BATTELLE NORTHWEST
BATTELLE MEMORIAL INSTITUTE
PACIFIC NORTHWEST LABORATORY
BATTELLE BOULEVARD, P. O. BOX 999, RICHLAND, WASHINGTON 99352

BNWL-1053

LEGAL NOTICE

PACIFIC NORTHWEST LABORATORY
RICHLAND, WASHINGTON
operated by
BATTELLE MEMORIAL INSTITUTE
for the
UNITED STATES ATOMIC ENERGY COMMISSION UNDER CONTRACT AT(45-1)-1830

AEC-RL RICHLAND, WASH.

BNWL-1053
UC-80,
Reactor Technology

REACTOR PHYSICS QUARTERLY REPORT
JANUARY, FEBRUARY, MARCH 1969

By

The Staff of
Reactor Physics Department
L. C. Schmid, Manager

Physics Research Department
E. D. Clayton, Manager

and

Reactor Physics and Operations
of the FFTF
R. E. Heineman, Manager

May 1969

BATTELLE MEMORIAL INSTITUTE
PACIFIC NORTHWEST LABORATORY
RICHLAND, WASHINGTON 99352

Printed in the United States of America
Available from
Clearinghouse for Federal Scientific and Technical Information
National Bureau of Standards, U.S. Department of Commerce
Springfield, Virginia 22151
Price: Printed Copy $3.00; Microfiche $0.65

REACTOR PHYSICS QUARTERLY REPORT
JANUARY, FEBRUARY, MARCH 1969

FORWARD

The objective of the Reactor Physics Quarterly Report is to inform the scientific community in a timely manner of the technical progress made on the many phases of reactor physics work within the laboratory. The report contains brief technical discussions of accomplishments in all areas where significant progress has been made during the quarter. The results presented herein should be considered preliminary, and do not constitute final publication of the work. A list of publications and papers issued during the last quarter is included in the report. Anyone desiring additional information concerning the work reported herein is encouraged to contact the author directly.

PREVIOUS REPORTS IN THIS SERIES

HW-42182	October, November, December	1955
HW-43441	January, February, March	1956
HW-44525	April, May, June	1956
HW-47012	July, August, September	1956
HW-48893	October, November, December	1956
HW-50598	January, February, March	1957
HW-51983	April, May, June	1957
HW-53492	July, August, September	1957
HW-54591	October, November, December	1957
HW-55879	January, February, March	1958
HW-56919	April, May, June	1958
HW-57861	July, August, September	1958
HW-59126	October, November, December	1958
HW-60220	January, February, March	1959
HW-61181	April, May, June	1959
HW-62727	July, August, September	1959
HW-63576	October, November, December	1959
HW-64866	January, February, March	1960
HW-66215	April, May, June	1960
HW-67219	July, August, September	1960
HW-68389	October, November, December	1960
HW-69475	January, February, March	1961
HW-70716	April, May, June	1961
HW-71747	July, August, September	1961
HW-72586	October, November, December	1961
HW-73116	January, February, March	1962
HW-74190	April, May, June	1962
HW-75228	July, August, September	1962
HW-76128	October, November, December	1962
HW-77311	January, February, March	1963
HW-77871	April, May, June	1963
HW-79054	July, August, September	1963
HW-80020	October, November, December	1963
HW-81659	January, February, March	1964
HW-83187	April, May, June	1964
HW-84369	July, August, September	1964
HW-84608	October, November, December	1964
BNWL-95	January, February, March	1965
BNWL-149	April, May, June	1965
BNWL-193	July, August, September	1965
BNWL-222	October, November, December	1965
BNWL-284	January, February, March	1966
BNWL-315	April, May, June	1966
BNWL-340	July, August, September	1966
BNWL-400	October, November, December	1966

BNWL-472	January, February, March	1967
BNWL-534	April, May, June	1967
BNWL-634	July, August, September	1967
BNWL-685	October, November, December	1967
BNWL-775	January, February, March	1968
BNWL-887	April, May, June	1968
BNWL-921	July, August, September	1968
BNWL-985	October, November, December	1968

TABLE OF CONTENTS

TABLE OF CONTENTS

FIGURES

TABLES

1.0 SUMMARY

REACTOR THEORY AND CODE DEVELOPMENT

The development of the Battelle Monte Carlo (BMC) code is completed. The BMC code is an improved version of the RBU Monte Carlo code and is written in FORTRAN V for use on the UNIVAC 1108 computer system. A number of test problems have been run successfully, and a code document is being written.

A computer code, KINPAR, has been written to aid in nuclear kinetic studies. The code, computes the ratio of effective delayed neutron fraction to the neutron lifetime, $\hat{\beta}/\ell$. Presently, the code utilizes output from the one-dimensional diffusion theory code, HFN, as input in computing this ratio. The code is being used in theory-experiment correlation studies.

A procedure permitting the resonance contributions of each resolved resonance to be allocated among several fine groups, instead of being restricted to a single fine group, has been developed and incorporated into the epithermal spectrum code HRG.

A digital computer code has been developed to analyze gamma-ray spectra to deduce intensities of the various gamma-ray photo peaks present. Initial applications have been made in studies of gamma-ray spectra from fission products in irradiated fuel, but the code is applicable in the analysis of gamma-ray spectra from any source.

A program Gas-I-A constructs analytic streamtube integrals for the supersonic flow of an ideal gas mixture through an open-loop or closed-loop succession of nozzles, oblique-shock diffusers, normal shocks, bypass flows with pressure-matched re-entries, heat exchangers, burners, turbines, compressors, shock pumps and other such elements simply characterizable in terms of mass, momentum, energy, or entropy transfer.

A general multigroup formulation has been derived for the theory of the PCTR experiments.

THERMAL REACTORS

Analytical correlations are being made of the Batch Core fueled experiment conducted in the PRCF and the PRTR. Quantities correlated are the foil activation traverses and coolant void coefficient in the PRCF experiment, and values of k_{eff}, boron worth, peripheral fuel worth and coolant worth in the PRTR initial critical experiment.

A comparison of exponential assembly measurements made using point detectors (indium foils) and finite-sized detectors (BF_3 chambers) has shown that the two methods yield the same results, within the experimental uncertainties. The comparisons were made in three lattices using Al–5 wt% Pu fuel and one lattice using UO_2–4 wt% PuO_2 fuel.

Measurements have been made in the PRCF of the reactor transfer function for a core loading of 19-rod clusters of UO_2–2 wt% PuO_2 rods in D_2O moderator. The measurements were accomplished by recording reactor noise with the assembly at delayed critical and analyzing the resulting recordings in the frequency domain. Results were obtained for three core sizes and associated boron concentrations in the moderator.

A detailed three-dimensional model for the MTR-Phoenix fuel loading has been developed. The model includes reflector penetration for beam tubes and structural materials. This is accomplished for two energy groups and in three dimensions with 28 by 18 by 39 mesh points.

A study of the sensitivity of k_{eff} to compositional uncertainties in critical assemblies has been made. The method is discussed for future reference and the results for the specific example give a ±1.6 mk variation for these compositional uncertainties.

The reactivity effects associated with improvements in slowing-down theory code HRG have been evaluated for some Al-Pu-H_2O systems.

CRITICAL MASS PHYSICS

A series of heterogeneous critical experiments were performed using PuO_2-polystyrene fuels at H/Pu ratios of 5 and 15 with depleted uranium (0.222 wt% ^{235}U) layers interspersed within the core regions. These data will provide an interim check on the accuracy of computational models and cross section data currently being used in survey calculations for homogeneous mixtures of PuO_2 and UO_2 typical of LMFBR fuels.

A series of pulsed neutron source measurements were made as part of a research effort to develop a capability for making "in-plant" reactivity evaluations in support of nuclear safety. Measurements were made on two different geometrical systems of the same material for which k_∞ had previously been measured in the PCTR. Good agreement was obtained between the k_∞ value for this material and the prompt neutron decay constants, in that both of these parameters yielded the same values for k_{eff}, within experimental accuracy.

Experiments have been performed on $Pu(NO_3)_4$ solutions with 18.4 wt% ^{240}Pu at a concentration of 66.5 g Pu/liter, using the expandable-slab critical assembly. Data were acquired for critical systems which were bare and laterally reflected with either water or a 1 in. thickness of Lucite. Analysis of the data yielded extrapolation lengths and bucklings which are a function of the configuration. It is suspected that the variations in buckling are due ultimately to the spatial dependence of the neutron flux spectrum within the thin slabs.

2.0 REACTOR THEORY AND CODE DEVELOPMENT

THE BATTELLE MONTE CARLO (BMC) CODE

D. H. Thomsen

Theoretical methods and analytical techniques utilized for reactor design are based upon the use of approximations and assumptions. Monte Carlo techniques are useful in evaluating the effects of assumptions and approximations on the accuracy of computed results. Frequently, these studies dictate the need for improvements in the design methods.

The RBU Monte Carlo code was developed for this purpose.[1] The code was written in machine language for use on the IBM-7090 digital computer. A more flexible and faster running code than RBU was desirable and became possible with the availability of the UNIVAC 1108 computer at the Hanford project. Thus the Battelle Monte Carlo (BMC) code[2] was developed.

The BMC code is an updated version of the RBU Monte Carlo code. The BMC code is coded in FORTRAN V for use on the UNIVAC 1108 computer system.

The BMC code uses many of the theories as formulated in the RBU Monte Carlo code. However, there are several major differences.

- Statistics are obtained as an integral part of the output.
- The batch method is used to obtain statistical samples instead of equilibrium and census times.
- The weight reduction method of accounting for absorption is used.
- Provisions were added for controlling the time spent in the thermal calculation to that spent in the epithermal calculation.
- The cross sections are obtained from the ENDF/B cross-section format.[3]

Coding of the BMC code and the BMC cross-section library code, BMCLIB, is complete. A number of test problems have been run, and testing continues. Details of the changes, input requirements, and output format are being documented.

References

1. *J. R. Triplett, E. T. Merrill and J. R. Burr. The RBU Reactor-Burnup Code: Formulation and Operating Procedures, HW-70049, Available from Clearinghouse for Federal Scientific and Technical Information, Springfield, Virginia, July 1961.*

2. *D. H. Thomsen. Reactor Physics Monte Carlo Applications, BNWL-SA-1513. Pacific Northwest Laboratory, Richland, Washington, September 20, 1967.*

3. *H. C. Honeck. ENDF/B - Specifications for an Evaluated Nuclear Data File for Reactor Applications, BNL-50066 (T-467). Brookhaven National Laboratory, Upton, New York, May 1966. (Revised July 1967 by S. Pearlstein)*

KINPAR

N. E. Carter and W. L. Purcell

An accurate prediction of the nuclear kinetic characteristics is important to the safety of reactor design. An important nuclear kinetic parameter is the ratio of effective delayed neutron fraction to the neutron lifetime, $\hat{\beta}/\ell$. To aid in kinetic studies, a computer code called KINPAR has been written for calculating this ratio.

The code uses standard perturbation theory expressions[1] for $\hat{\beta}$ and ℓ. The code in its present form utilizes information (such as direct and adjoint fluxes) obtained from a one-dimensional diffusion theory solution (code HFN)[2] to the problem to perform the calculation of $\hat{\beta}/\ell$. Modifications were made to routines of HFN to manipulate the data necessary for KINPAR. The KINPAR problem directly follows the HFN problem.

The code is presently being used in studies of analytically correlating measured values of $\hat{\beta}/\ell$.[3]

References

1. *S. R. Long. "Fast Neutron Power Reactor Studies with ZPR-III," Proceedings of the Second United Nations International Conference on the Peaceful Uses of Atomic Energy, vol. 12. 1958.*

2. *J. R. Lilley. Computer Code HFN - Multigroup, Multi-region Neutron Diffusion Theory in One Dimension. HW-71545. Available from Clearinghouse for Federal Scientific and Technical Information, Springfield, Virginia.*

3. *D. L. Prezbindowski and M. A. Mannan. "Theoretical Correlation of the PRTR Batch Core Experiment," Plutonium Utilization Program Technical Activities Quarterly Report, September, October, November 1968, BNWL-963. Pacific Northwest Laboratory, Richland, Washington, January 1969. (and also see this quarterly).*

THE ALLOCATION OF RESONANCE CONTRIBUTIONS TO FINE GROUPS IN HRG

J. L. Carter

According to the GAM-I procedure used in HRG for treating resonances, the effective cross section for each resolved resonance is allocated to the fine group in which the resonance energy lies. For a broad, strong resonance, this excessive concentration of absorption in a single fine group, and the resulting excessive depression of the fine group flux, is an inaccurate approximation of the true situation. To remedy this, the scheme described below for allocating the effective cross section of a resonance among several fine groups has recently been included in HRG. The effect of this change can be significant, since both the 6.7 eV resonance of ^{238}U and the 1.06 eV resonance of ^{240}Pu are examples of such a resonance. To illustrate, resonance absorption increases of about 5% in ^{238}U and 10% in ^{240}Pu and a reactivity decrease of about 25 milli-k were calculated for a representative light water lattice containing mixed oxide fuel with 2 wt% PuO_2 containing 8% ^{240}Pu.

The effective cross section for a reaction process for fine group n can be written as

$$\sigma_{n,eff} = \frac{\int_n dE\ \sigma(E)\ \phi_{reg}(E)}{\int_n dE\ \phi_{cell}(E)} \qquad (1)$$

where it has been implicitly assumed that the isotope involved in the reaction is in a region characterized by flux $\phi_{reg}(E)$, the homogenized cell flux is $\phi_{cell}(E)$, and the homogenized and lumped nuclear densities for the isotope are related so that $N_{reg}\ V_{reg}/N_{cell}\ V_{cell} = 1$. Now for a resonance, Equation (1) can be written as

$$\sigma_{n,eff} = \frac{\int_{res} dE\ \sigma(E)\,\phi_{reg}(E)}{\int_n dE\ \phi_{cell}(E)} \cdot \frac{\int_n dE\ \sigma(E)\,\phi_{reg}(E)}{\int_{res} dE\ \sigma(E)\,\phi_{reg}(E)}$$

$$= \frac{RI}{\int_n dE\ \phi_{cell}(E)} \cdot F_n \qquad (2)$$

where the factor F_n can be interpreted as the fraction of the resonance integral to be allocated to fine group n. In this interpretation, the GAM-I procedure has been to set $F_n = 1$ if the resonance energy lies in n, but set it zero otherwise. The revised procedure to evaluate F_n in HRG is to homogenize the flux by an equivalence principle which approximates the collision probability by the Wigner rational approximation and to use unbroadened cross sections. Then, specifying the capture cross section for illustration, and using the usual notation,[1] the general form of the integrals involved in F_n can be written as

$$\int_{E_1}^{E_2} \sigma_\gamma(E)\ \phi_{reg}(E)\ dE = \frac{\sigma_o\ \Gamma_\gamma\ \beta_e}{2E_o} \int_{x_1}^{x_2} \frac{\psi}{\psi + \beta_e}\ dx \qquad (3)$$

where

$$\psi = (1 + x^2)^{-1}, \text{ with } x = 2(E - E_o)/\Gamma$$

$$\beta_e = \frac{(1 - \lambda)\ \sigma_m + \lambda\sigma_p + \sigma_e}{\sigma_o} \cdot \frac{\Gamma}{\Gamma_\gamma + \lambda\Gamma_n}$$

$$\sigma_e = 1/N_{reg}\bar{\ell}, \text{ with } \bar{\ell} = \text{effective average chord length,}$$

and $\lambda = 0$ or 1 for IM or NR approximation, respectively.

Equation (3) can be evaluated analytically to give

$$\int_{E_1}^{E_2} \sigma_\gamma(E)\ \phi_{reg}(E)\ dE = \frac{\sigma_o\ \Gamma_\gamma}{2E_o}\sqrt{\frac{\beta_e}{1 + \beta_e}}\left(\tan^{-1}\sqrt{\frac{\beta_e}{1 + \beta_e}}\ x_2 - \tan^{-1}\sqrt{\frac{\beta_e}{1 + \beta_e}}\ x_1\right) \qquad (4)$$

The integration limits for F_n are the group boundaries of fine group n and the entire energy range for the numerator and denominator integrals, respectively, giving

$$F_n = \frac{1}{\pi}\left(\tan^{-1}\sqrt{\frac{\beta_e}{1 + \beta_e}}\ x_{n-1} - \tan^{-1}\sqrt{\frac{\beta_e}{1 + \beta_e}}\ x_n\right) \qquad (5)$$

Although in principle this method gives a contribution to every fine group, in practice some cutoff procedure is needed. For this purpose, two energies equally distant from E_o are selected such that they include between them a specified fraction of the resonance integral as given by Equation (4); this fraction has arbitrarily been chosen as 0.9. The fine groups containing these two energies are then determined, and the resonance integral is allocated to these and all intermediate groups, with the contributions beyond the cutoff energies included in the bounding groups. No additional input to HRG is required. In the illustrative calculations quoted earlier, this procedure allocated the 6.7 eV ^{238}U resonance to four fine groups and the 1.06 eV ^{240}Pu resonance to three.

The F_n depend on geometry and the scattering properties of the admixed moderator through β_e. Because unbroadened cross sections are used, the F_n are not dependent on the temperature. To check on the validity of neglecting temperature dependence, a series of calculations was made for the 1.06 eV resonance of ^{240}Pu for a range of scattering cross sections per absorber atom and temperatures from 300 to 1200 °K. The code NIT, which uses the ZUT[2] procedure for calculating resonance integrals and allocates the contributions to the GAM-I fine group structure, was used for this check. The very slight temperature dependence found for these allocations confirms that it can reasonably be neglected.

The calculation of $\sigma_{n,eff}$ from Equation (2) also requires the evaluation of $\int_n dE\ \phi_{cell}(E)$. The evaluation of this integral in HRG has been described previously.[3] However, some minor inconsistencies between the assumptions used to evaluate F_n and those of Reference 3 made it desirable to modify slightly the calculation of the flux integral. In terms of the present notation, the flux integral becomes

$$\int_n \phi_{cell}(E)\, dE = \int_{E_n}^{E_{n-1}} \frac{dE}{E} - \frac{N_{cell}}{N_{reg}} \cdot \frac{\Gamma}{2E_o} \int_{x_n}^{x_{n-1}} \frac{\psi}{\psi + \beta_e}\, dx$$

$$= 0.25 - \frac{N_{cell}}{N_{reg}} \cdot \frac{\Gamma}{2E_o \sqrt{\beta_e(1 + \beta_e)}} \cdot \pi F_n \qquad (6)$$

Equation (6) is now being used in HRG.

References

1. *G. D. Joanou and J. S. Dudek. GAM-I: A Consistent P1 Multigroup Code for the Calculation of Fast Neutron Spectra and Multigroup Constants, GA-1850. General Atomics Division, General Dynamics Corp., San Diego, California, 1961.*

2. *G. F. Kuncir. A Program for the Calculation of Resonance Integrals, GA-2525. General Atomics Division, General Dynamics Corp., San Diego, California, 1961.*

3. *J. L. Carter. "Effective Cross Sections for Resonances in HRG," Reactor Physics Quarterly Report, July, August, September 1966, BNWL-340. Pacific Northwest Laboratory, Richland, Washington, October 15, 1966.*

ANALYSIS OF GAMMA-RAY SPECTRA BY DIGITAL COMPUTER TECHNIQUE

G. D. Seybold

The problem of using high-resolution spectral data from fission-product gamma rays to infer fuel burnup is under study at PNL. An essential part of the solution to this problem is a means of obtaining realistic determinations of the intensities of the various gamma-ray photopeaks from the fission products of interest. A computer program has been developed which performs this portion of the analysis.

Programs General Capabilities

Program GSSLRN is a photon spectrum analysis code written in Fortran V for the UNIVAC 1108, which examines the digitized

data from a multichannel analyzer, searches for and locates the photopeaks present, fits each photopeak with an analytic function (Gaussian (s) + exponential), test each fitted peak against statistical criteria such as the full-width at half-maximum, and integrates the resolved area under each photopeak to yield the intensity for that peak. Multiplets with mean values considerably closer than their fitted full-widths-at-half-maximum would normally allow can be identified and resolved, including small intensity peaks lying under the wings of larger peaks. The mean energies and their errors for each peak and intensities are also determined. The program is still under development, but has proven to be highly successful with spectral data from fuel irradiated in the EBWR.

Program Specifics

Program GSSLRN has been written using the fitting logic of program LEARN[1] as the heart of its analysis. The intent is to apply the most stringent statistics available, using the second order Taylor expansion techniques as they are applied in the Newton-Raphson iteration method.

The program is directed toward the problem of resolving multiplets which can be very closely coupled. The resolution of Gaussians implies that the theoretical function can be recursive for the assumed Gaussian shapes. The analytical function is of the form

$$Y = A_1 e^{A_2 \left(x_m - x_1\right)} + \sum_{i=3,JJ,3}^{JJ=32} A_i \cdot \exp\left[-1/2 \left(A_{i+1} X_m - A_{i+2}\right)^2 \right]$$

where A_1 = amplitude of the exponential background,
A_2 is a parameter defining the slope of the background exponential,

A_i is the amplitude of the symmetric part of each Gaussian,

$A_{i+1} = \frac{1}{\sigma}$ for each Gaussian, and

$A_{i+2} = \overline{X}/\sigma$ where $\overline{X}$ is the mean energy or channel number, and

σ = FWHM/2.355 for each Gaussian.

Because of the recursive properties of the theoretical function, it is possible to obtain up to ten Gaussian-fitted shapes in multiplet form characterizing a "set." This method has proven to be successful and allows the analysis of resolved Gaussians to be more complete.

Currently, GSSLRN uses a peak-searching technique,[2] which tends to be overly conservative. This technique tends to locate false peaks in addition to those which really exist. The logic coded into GSSLRN, along with the regression analysis in LEARN,[1] has proven successful in eliminating false peaks. In addition, the analysis has shown that unresolved photopeaks can be located and resolved with good statistical determination. This technique has been applied to high as well as low intensity spectra.

Input for GSSLRN

Except for the photopeak spectra, the input required for executing the code can be put on one or two cards.

The major options available are the following:

1. Execution with no plotting
2. Same as (1) except with uncertainties for all data being printed
3. Execution with computer plots
4. Execution with CALCOMP plots.

One can expect that the execution time using (3) would be approximately 3.25 sec per peak on the average. This average

includes trying to analyze false peaks referred to earlier. Presently, an additional 20 sec is required for initial allocation within the computer, making the total processing time approximately (20 + 3.25 N) sec.

References

1. *B. H. Duane. Maximum Likelihood Nonlinear Correlated Fields (BNW Program LIKELY), BNWL-390. Pacific Northwest Laboratory, Richland, Washington, September 1967.*

2. *M. A. Mariscotti. "A Method for Automatic Identification of Peaks in the Presence of Background and Its Application to Spectrum Analysis," Nucl. Instr. Methods, pp. 309-320. 1967.*

IDEAL GAS FLOW WITH MASS, MOMENTUM, ENERGY, AND ENTROPY TRANSFER (Battelle-Northwest Program GAS-I-A)

B. H. Duane

Machine Analysis Abstract

Battelle-Northwest Program Gas-I-A constructs analytic streamtube integrals for the supersonic flow of an ideal gas mixture through an open-loop or closed-loop succession of nozzles, oblique-shock diffusers, normal shocks, bypass flows with pressure-matched re-entries, heat exchangers, burners, turbines, compressors, shock pumps, and other such elements simply characterizable in terms of mass, momentum, energy, or entropy transfer.

Physics Representation

Mass Imbalance: $\nabla \cdot \rho \underline{v} = Q_1$

Energy Imbalance: $\nabla \cdot \rho \underline{v}(h + v^2/2) = Q_2$

Momentum Imbalance: $\nabla \cdot (\rho \underline{vv} + p) = \underline{Q}_3$

Entropy Imbalance: $\nabla \cdot \rho \underline{v} s = Q_4$

Here ρ is fluid density, $\underline{v}$ is flow velocity, T is fluid temperature, p is fluid pressure, $r = p/\rho T$ is the gas constant, c_v is specific heat/mass at constant volume, $h = (c_v + r)T$ is fluid enthalpy/mass, and $s = s_o - r \ln \rho + c_v \ln T$ is fluid entropy/mass. The flexible source-sinks Q_1, Q_2, $\underline{Q}_3$, and Q_4 provide for piecewise uniform transfer of mass, energy, momentum, and entropy, respectively.

These equations are integrated analytically over each streamtube segment by conversion to surface integrals, to provide firm numeric reliability for any segmentation mesh size. Traveling oblique shocks are generated as Galilean velocity transforms of static normal shocks.

ON THE THEORY OF PCTR EXPERIMENTS

D. D. Lanning

The derivation of the theory of PCTR experiments in terms of the general multigroup formulation has been discussed many times in the past. Previous work has been done both in two and three group formulations. Recently, R. E. Heineman suggested that the use of the standard calculational trick of solving for an effective $\bar{\nu}$ might resolve the general multigroup problem. The following deviation includes the theory of PCTR experiments in a general multigroup formulation that leads to the derivation in the measured result due to a mismatch between the flux in the PCTR and the proper equilibrium flux.

Consider the i^{th} group diffusion equation for a multigroup formulation:

$$D_i \nabla^2 \phi_i + \sum_j (w_{ij} \Sigma_j^o - \delta_{ij} \Sigma_j^a) \phi_j + \sum_j \chi_{ij} \Sigma_j^f \nu_j \phi_j = 0$$

where

$$\delta_{ij} = 0 \quad ,$$

and

$$\delta_{ii} = 1 \quad .$$

w_{ij} is the fraction of neutrons scattered from group j and deposited in group i.

w_{ii} = -1 is the loss of neutrons from group i by out-scattering.

χ_{ij} is the fraction of neutrons produced by fissions in the j^{th} group that are deposited by the fission distribution into the i^{th} group.

ν_j is the neutrons produced per fission induced from j^{th} group neutrons.

The multigroup balance of the group-to-group scattered neutrons becomes:

$$\sum_{ij} w_{ij} \Sigma^{o}_{j} \phi_j = 0$$

The sum over i and j of the multigroup equation becomes:

$$\sum_{i} D_i \nabla^2 \phi_i + \sum_{ij} (\chi_{ij} \Sigma^{f}_{j} \nu_j - \delta_{ij} \Sigma^{a}_{j}) \phi_j = 0$$

or in terms of a matrix element M_{ij},

$$D_i \nabla^2 \phi_i + \sum_{j} M_{ij} \phi_j = 0 \quad ,$$

$$M_{ij} = w_{ij} \Sigma^{o}_{j} + \chi_{ij} \Sigma^{f}_{j} \nu_j - \delta_{ij} \Sigma^{a}_{j} \quad ,$$

$$\sum_{ij} M_{ij} \phi_j = \sum_{ij} (\chi_{ij} \Sigma^{f}_{j} \nu_j - \delta_{ij} \Sigma^{a}_{j}) \phi_j \quad .$$

Taking the definition of k_∞ to be

$$k_\infty = \frac{\text{Total Production of Neutrons/Sec}}{\text{Total Absorption of Neutrons/Sec}} \quad ,$$

Then,

$$k_\infty = \frac{\sum_{ij} \chi_{ij} \Sigma^{f}_{j} \nu_j \phi_j}{\sum_{ij} \delta_{ij} \Sigma^{a}_{j} \phi_j} \quad .$$

Experience has shown that the criticality condition is best studied by making effective changes in ν. This leaves the proper balance on the group to group transfer and tends to keep the proper energy equilibrium distribution. Hence, it is convenient to write:

$$\sum_{ij} M_{ij} \phi_j = \sum_{ij} \chi_{ij} \Sigma^{f}_{j} \nu_j \phi_j \left(1 - \frac{1}{k_\infty}\right) \quad ;$$

or,

$$\sum_{ij} M_{ij}\phi_j = \bar{\nu}\left(\frac{k_\infty - 1}{k_\infty}\right) \sum_{ij} \chi_{ij} \Sigma_j^f \frac{\nu_j}{\bar{\nu}} \phi_j$$

where,

$\bar{\nu}$ is the average value of ν_j

$$\bar{\nu} = \frac{\sum_j \Sigma_j^f \phi_j \nu_j}{\sum_j \Sigma_j^f \phi_j} \quad .$$

Consider the PCTR type of experiment in which $k_\infty = 1$. The attempt is to match the spectrum on the central cell, and find the proper cell conditions to make $k_\infty = 1.000$. If $k_\infty' = 1.000$ in the measured result, the prime indicating the PCTR measured condition, the question to be asked here is: what is the error due to a mismatch in the neutron spectrum incident upon the central cell? This question has been answered in both two and three group formulations, but never in a complete multigroup formulation.

The measurement in the PCTR consists of simultaneously determining the matched spectrum incident on the central cell and the proper central cell constituents such that the change in the PCTR reactivity is zero when the central cell is removed leaving a void. The k_∞ of the void as seen by the PCTR is unity. With no change in neutron distribution or reactivity upon re-insertion of the central cell, the k_∞ of the central cell material is thus implied to be unity.

From a theoretical point of view, both the equilibrium; i.e., perfectly matched, condition and the PCTR condition can be calculated and the error due to a spectral mismatch in the PCTR is thus evaluated.

The proper equilibrium comes from the critical assembly of the central cell constituents. In this case with k_∞ equal to unity, there is no leakage ($D_i \nabla^2 \phi_i = 0$); hence,

$$\sum_j M_{ij} \phi_j = 0, \text{ and } k_\infty - 1 = 0 \quad .$$

Similarly, for the adjoint equation,

$$\sum_j M_{ij}^\dagger \phi_j^\dagger = 0 \quad .$$

It is important to note for future reference that in this case:

$$\sum_i \phi_i^\dagger M_{ij} = \sum_j M_{ij}^\dagger \phi_j^\dagger = 0 \quad .$$

In the core of the PCTR the measured quantity is the change in reactivity between cell-in and cell-out ($\Delta\rho_{cell}$), and the experiment is satisfied when:

$$\Delta\rho_{cell} = 0.$$

If the reactor is just critical before the central cell is inserted, it remains critical after the central cell is inserted:

Before: $$D_i \nabla^2 \phi_i' + \sum_j M_{ij}^R \, _j = 0$$

After: $$D_i \nabla^2 \phi_i'' + \sum_j (M_{ij}^R + M_{ij}') \phi_j'' = 0$$

where M_{ij}' is the change in the matrix operator due to the addition of the central cell and only exists over the volume of the central cell. Since the experiment consists of assuring that the flux is simultaneously matched at the time $\Delta\rho_{cell} = 0$, then within the experimental uncertainty $\phi'' = \phi'$ and $\phi^{\dagger''} = \phi^{\dagger'}$ throughout the reactor, which means that the standard perturbation equation is exact in this case within the experimental

uncertainty. Multiplying the above equation by $\phi_i^{\dagger'}$, summing over i, and integrating over the volume of the whole reactor gives:

$$\sum_{ij} \phi_i^{\dagger'} M'_{ij} \phi'_j = 0$$

where the volume of the central cell is cancelled out since $\phi_i^{\dagger'}$ and ϕ'_i are both the flat adjoint and flux values found in the void before the central cell is inserted.

Recall that the proper cell constituents to make $k_\infty = 1.000$ give the matrix element M_{ij}, while the measured cell constituents give the measured matrix elements M'_{ij}. The i^{th} group error in the measurement is expressed as:

$$\delta M_{ij} = M'_{ij} - M_{ij} \quad .$$

Assembling all of the above equations leads to the important result as follows:

$$\sum_{ij} \phi_i^{\dagger'} M'_{ij} \phi'_j = \sum_{ij} \phi_i^{\dagger'} (M_{ij} + \delta M_{ij}) \phi'_j = 0 \quad .$$

This gives:

$$- \sum_{ij} \phi_i^{\dagger'} \delta M_{ij} \phi'_j = \sum_{ij} \phi_i^{\dagger'} M_{ij} \phi'_j \quad .$$

Next, note that:

$$\sum_{ij} (\phi_i^{\dagger'} - \phi_i^{\dagger}) M_{ij} (\phi'_j - \phi_j) \equiv \sum_{ij} \delta\phi_i^{\dagger} M_{ij} \delta\phi_j =$$

$$- \sum_{ij} \phi_i^{\dagger} M_{ij} \delta\phi_i - \sum_{ij} \delta\phi_i^{\dagger} M_{ij} \phi_j + \sum_{ij} \phi_i^{\dagger'} M_{ij} \phi'_j \quad ;$$

and since $\sum_i \phi_i^{\dagger} M_{ij} = 0$, and $\sum_j M_{ij} \phi_j = 0$,

then $$\sum_{ij} \phi_i^{\dagger'} M_{ij} \phi'_j = \sum_{ij} \delta\phi_i^{\dagger} M_{ij} \delta\phi_j$$

with the concluding result that: The error in the matrix δM_{ij} can be related to the error in the group fluxes, $\delta\phi$; (i.e., the difference between the PCTR central cell group fluxes ϕ_i', and the equilibrium system group fluxes ϕ_i) by the expression:

$$\sum_{ij} \phi_i^{\dagger\prime} \delta M_{ij} \phi_j' = - \sum_{ij} \delta\phi_i^{\dagger} M_{ij} \delta\phi_j$$

One way to utilize this expression is to use the effective change in $\bar{\nu}$. Let $\bar{\nu}' = \bar{\nu} + \delta\bar{\nu}$;
then,

$$\delta M_{ij} = M_{ij}' - M_{ij} = \frac{\bar{\nu}' - \bar{\nu}}{\bar{\nu}} (\chi_{ij} \textstyle\sum_j^f \nu j) \quad ,$$

where the group-to-group transfer cross sections and the absorption cross sections cancel. Substituting for δM_{ij} gives:

$$\frac{\bar{\nu}' - \bar{\nu}}{\bar{\nu}} = \frac{\delta\nu}{\nu} = \frac{\sum_{ij} \delta\phi_i^{\dagger} M_{ij} \delta\phi_j}{\sum_{ij} \phi_i^{\dagger\prime} \chi_{ij} \sum_j^f \nu_j \phi_j'}$$

In this case with $k_\infty = 1.000$ the relation holds:

$$\frac{\delta\nu}{\nu} = \frac{k_\infty' - k_\infty}{k_\infty} = \frac{\delta k_\infty}{k_\infty} \quad ,$$

where δk_∞ is the error in the measured value.

In summary, these expressions show that the error in the measured value of k_∞ due to the mismatch of the neutron spectrum, relative to the equilibrium spectrum, is proportional to the sum of the multigroup products of the mismatch in the flux and adjoints weighted by the matrix elements

$$M_{ij} = w_{ij} \textstyle\sum_j^o + \chi_{ij} \sum_j^f \nu j - \delta_{ij} \sum_j^a \quad .$$

APPENDIX

A test of the general multigroup formulation is provided by reducing to two-group theory and algebraically rearranging terms to see if the general equation reproduces the previous two-group result.

In the simple two-group case,

$$M_{11} = -(\Sigma_1^{rem} + \Sigma_1^{a}) \qquad \chi_{11} = 0$$

$$M_{12} = +\nu\Sigma_2^{f} \qquad \chi_{12} = 1$$

$$M_{21} = +\Sigma_1^{rem} \qquad \chi_{21} = 0$$

$$M_{22} = -\Sigma_2^{a} \qquad \chi_{22} = 0$$

$$\frac{M_{11}}{M_{12}} = -\frac{\phi_2}{\phi_1} \qquad \frac{M_{21}}{M_{22}} = -\frac{\phi_2}{\phi_1}$$

$$\frac{M_{11}}{M_{21}} = -\frac{\phi_2^{\dagger}}{\phi_1^{\dagger}} \qquad \frac{M_{12}}{M_{22}} = -\frac{\phi_2^{\dagger}}{\phi_1^{\dagger}}$$

$$-\frac{\delta\nu}{\nu} = \frac{\delta\phi_1^{\dagger}M_{11}\,\delta\phi_1 + \delta\phi_1^{\dagger}M_{12}\,\delta\phi_2 + \delta\phi_2^{\dagger}M_{21}\,\delta\phi_1 + \delta\phi_2^{\dagger}M_{22}\,\delta\phi_2}{\phi_1^{\dagger\prime}\nu\Sigma_2^{f}\phi_2'}$$

Since $\nu\Sigma_2^{f} = M_{12}$, the values of M_{ij} in the numerator can be divided by M_{12} and then the appropriate flux ratios can be substituted for the $\frac{M_{ij}}{M_{12}}$ ratios. By also changing $\delta\phi_i$ back to $\phi_i' - \phi_i$, etc., the equation becomes:

$$-\frac{\delta\bar{\nu}}{\bar{\nu}} = \frac{-\left(\phi_1^{\dagger\prime}-\phi_1^{\dagger}\right)\left(\phi_2/\phi_1\right)\left(\phi_1'-\phi_1\right)}{\phi_1^{\dagger\prime}\,\phi_2'} + \frac{\left(\phi_1^{\dagger\prime}-\phi_1^{\dagger}\right)\left(\phi_2'-\phi_2\right)}{\phi_1^{\dagger\prime}\,\phi_2'}$$

$$+\frac{\left(\phi_2^{\dagger\prime}-\phi_2^{\dagger}\right)\left(\frac{\phi_2}{\phi_1}\,\frac{\phi_1^{\dagger}}{\phi_2^{\dagger}}\right)\left(\phi_1'-\phi_1\right)}{\phi_1^{\dagger\prime}\,\phi_2} - \frac{\left(\phi_2^{\dagger\prime}-\phi_2^{\dagger}\right)\left(\frac{\phi_1^{\dagger}}{\phi_2^{\dagger}}\right)\left(\phi_2'-\phi_2\right)}{\phi_1^{\dagger\prime}\,\phi_2}$$

On expanding the equation and rearranging terms, the desired result is obtained:

$$\boxed{\frac{\delta\bar{\nu}}{\bar{\nu}} = -\frac{\left(\frac{\phi_1'}{\phi_2'}-\frac{\phi_1}{\phi_2}\right)}{\frac{\phi_1}{\phi_2}}\cdot\frac{\left(\frac{\phi_2^{\dagger\prime}}{\phi_1^{\dagger\prime}}-\frac{\phi_2^{\dagger}}{\phi_1^{\dagger}}\right)}{\frac{\phi_2^{\dagger}}{\phi_1^{\dagger}}}}$$

This is essentially the same as the previously derived result,[1]

$$\frac{\delta k_\infty}{k_\infty} = -\frac{\left(\frac{\phi_1'}{\phi_2'}-\frac{\phi_1}{\phi_2}\right)\left(\frac{\phi_1^{\dagger\prime}}{\phi_2^{\dagger\prime}}-\frac{\phi_1^{\dagger}}{\phi_2^{\dagger}}\right)}{\frac{\phi_1}{\phi_2}\qquad\frac{\phi_1^{\dagger}}{\phi_2^{\dagger}}}$$

That is, the error in k_∞ is equal to the product of the fractional mismatch in the fast to thermal ratios of the flux and adjoint. The inversion of the adjoint ratios between the two results is presumably due to the difference between considering the change in $\bar{\nu}$ (as done in the new derivation), or the change in Σ_2^a, as was the case in the earlier derivation. This difference will make very little change in any numerical evaluation.

---

1. *D. J. Donahue, et al. "Determination of k_∞ from Critical Experiments with the PCTR,"* Nucl. Sci. Eng., *vol. 4, p. 297. 1958.*

3.0 REACTOR PHYSICS

THEORETICAL CORRELATION OF THE PRTR BATCH CORE EXPERIMENT

M. A. Mannan* and D. L. Prezbindowski

Introduction

A detailed theoretical analysis is being made of the Batch Core fuel experiments conducted in the Plutonium Recycle Critical Facility (PRCF)[1] and the Plutonium Recycle Test Reactor (PRTR).[2] The purpose of the analysis is to determine the limitations of certain calculational methods in their application to predicting the behavior of the PRTR Batch Core Experiment and more fundamentally in their application to predicting the behavior of plutonium fueled thermal reactor systems. The calculational methods selected for this analysis are HTH[3] and HAMMER[4] multigroup cross section codes and the HFN,[5] FLOG,[4] EXTERMINATOR,[6] 2DB,[7,8] PERT4,[9] and KINPAR[10] reactor codes. The results of the analysis will provide a basis for selecting methods appropriate to the calculation of the PRTR Batch Core Experiments and identify those areas in which further theoretical development is required.

Calculational methods and results of the analysis of the PRCF critical experiments were reported earlier.[11] This report contains results of a theory-experiment correlation of the axial and radial flux traverse, the coolant void coefficient, and the worth of a peripheral fuel element in the PRCF. It further contains some values of the effective multiplication factors, k_{eff}, loss of coolant coefficients, boron coefficients, and the worth of a peripheral element in the critical experiments conducted in the PRTR.

---

* *On assignment to PNL under an International Atomic Energy Agency Fellowship.*

PRCF Critical Experiments

The gold foil activation traverses in the 13-element PRCF core with 4.64 wppm ^{10}B in the moderator were calculated using EXTERMINATOR(R-Z). The experimental and calculated axial and radial traverses are given in Figures 3.1 and 3.2 respectively. As shown in both figures, the results of the correlations in the active core regions are quite good. However, there are serious discrepancies in the reflector regions. The calculated values are much higher than the experimental values in the radial reflector and the bottom reflector region.

There are a number of aspects of the experimental procedure and the analytical correlation of experimental traverses that are inconsistent.

1) The moderator level used in the bare axial and radial irradiation was 2.25 in. higher than used in the just critical experiment. This increased moderator level compensated the negative worth of the foils and foil holders, but the calculated activation was obtained using fluxes from the standard critical experiment calculations. However, this difference in moderator level does not affect the activation rates in the radial direction nor in the bottom reflector region.
2) As shown in Figure 3.3, the radial foil holding tube passes near a control assembly and a safety rod guide tube. The absorption due to the safety rod guide tube is relatively smaller than that of a control rod assembly. The absorption difference causes an asymmetry in the activation traverse in the reflector region. The calculated traverse was obtained by calculating a core without a control rod assembly and by homogenizing the safety rod guide tube with the reflector. Furthermore, the usual radial symmetry condition was assumed in the calculation.

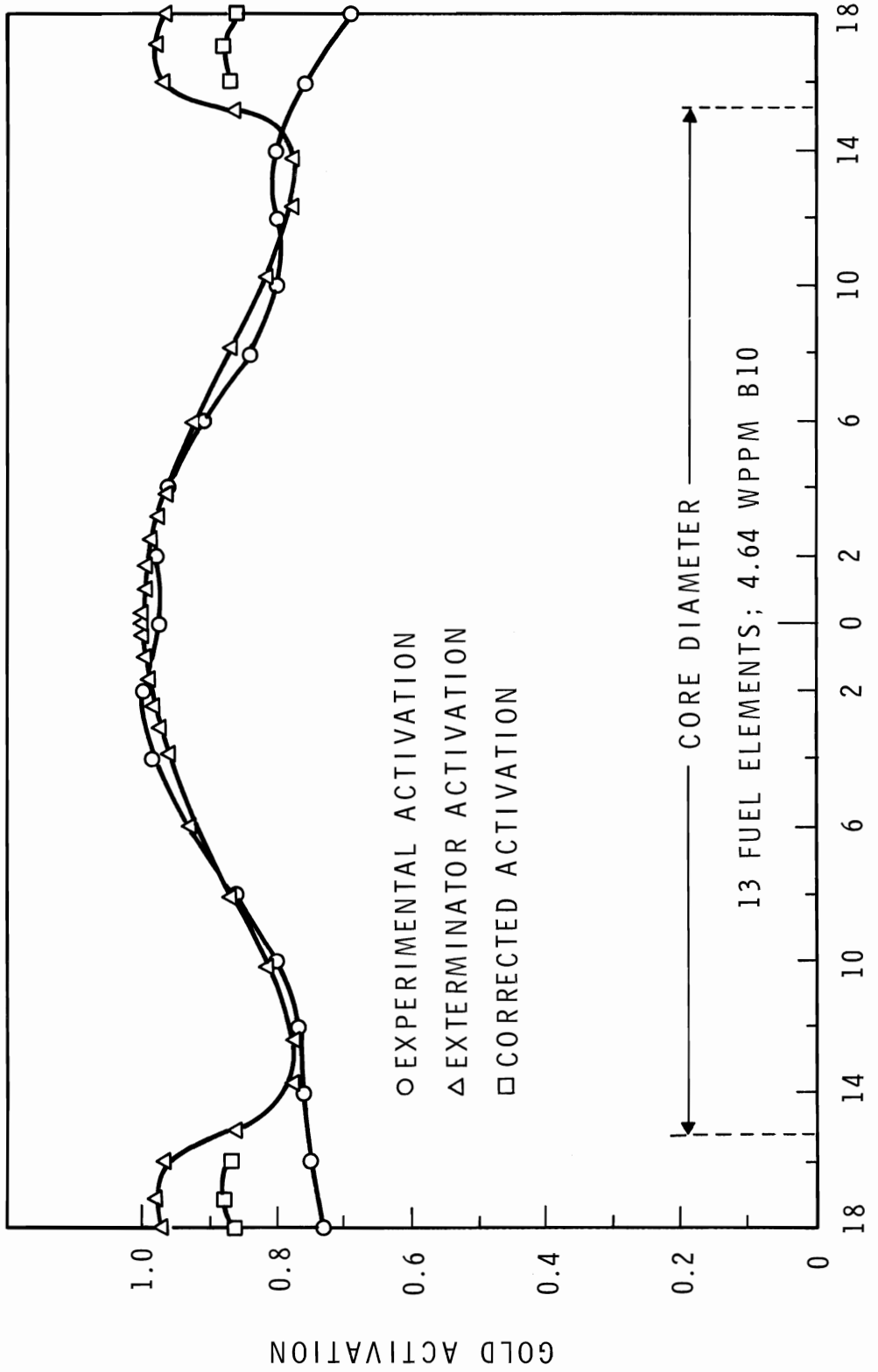

FIGURE 3.1. Comparison of Calculated and Experimental Radial Activation Traverses for the 13 Element Core

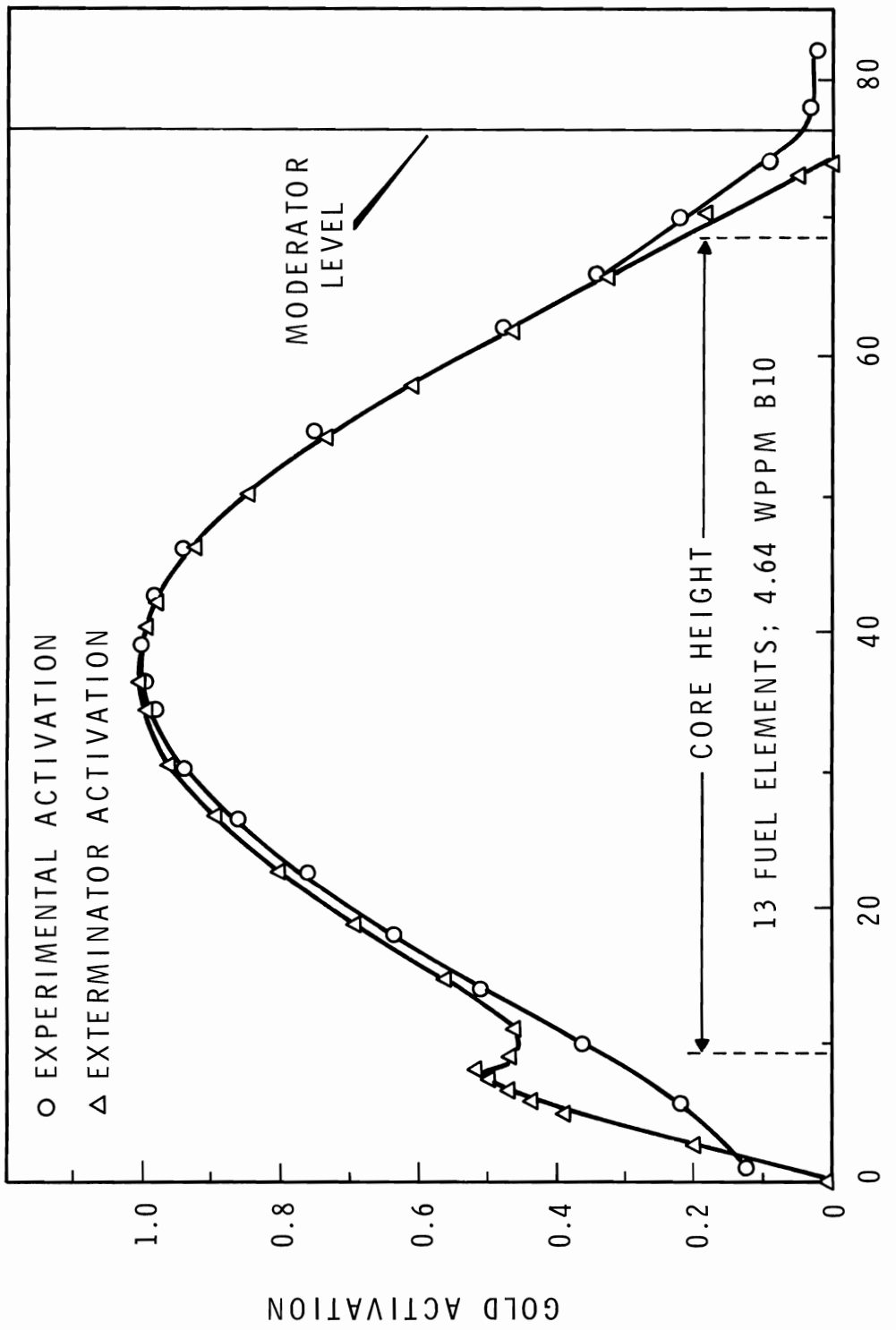

FIGURE 3.2. Comparison of Calculated and Experimental Axial Activation Traverses for the 13 Element Core

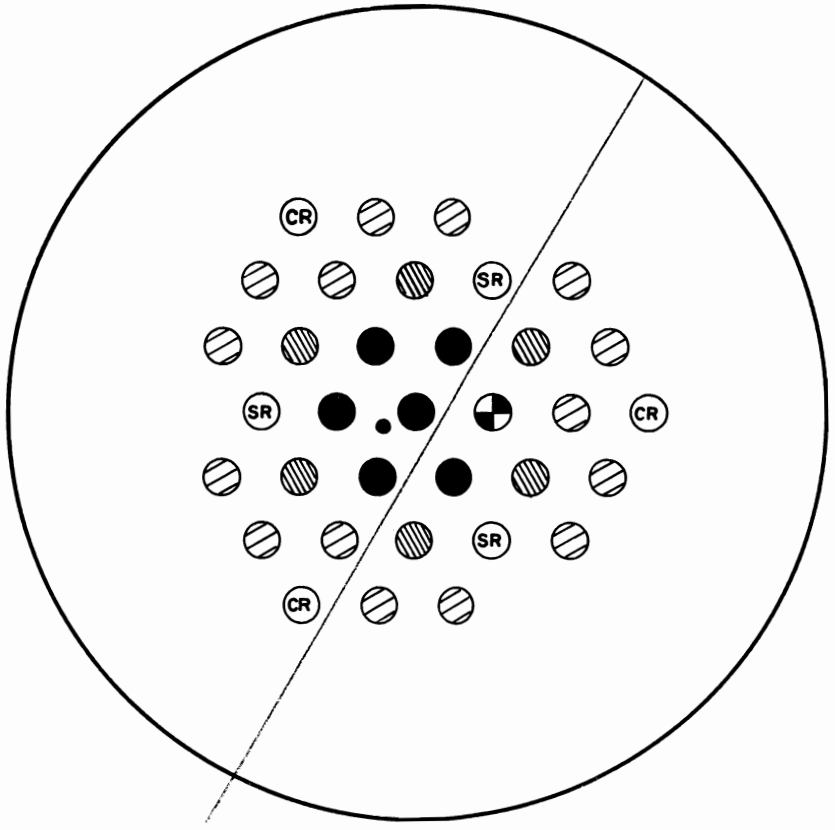

HORIZONTAL TRAVERSE MECHANISM

- INITIAL CRITICAL LOADING (6)
- ADDED TO FORM 7 ELEMENT
- ADDED TO FORM 13 ELEMENT
- ADDED TO FORM 28 ELEMENT
- (CR) CADMIUM CONTROL RODS
- (SR) CADMIUM SAFETY RODS
- VERTICAL TRAVERSE POSITION

FIGURE 3.3. Critical Assembly Configurations

3) The foil holding tube for the radial traverse was placed in the middle of the moderator region between fuel elements (Figure 3.3). In this position, the fluxes seen by detector foils within the active core region near the reflector are not too different from the fluxes in the adjacent reflector, and the experimental traverse shows little peaking in the reflector. A homogeneous core with cell-averaged parameters is used in the calculation. Therefore, fluxes obtained are cell-average fluxes. In the homogenized core model, there is a discontinuity in the absorption cross section at the core-reflector interface. Therefore, the calculated gold activity traverse has a large peak in the reflector. A simple correction for the heterogeneity effect was applied to the calculated flux traverses in the reflector region. The calculated values are multiplied by the ratio of the average thermal flux in the cell to the average thermal flux in the moderator of the cell obtained from THERMOS calculations. As shown in Figure 3.2, corrections to the activation decreases the discrepancy between the calculated and experimental traverses in the reflector region, but a substantial discrepancy still remains. The calculated axial traverse in the bottom reflector shows a peak which is not seen experimentally as was the case with radial reflector. This overestimation of calculated thermal fluxes in the reflector regions undoubtedly contributes to the overestimation of k_{eff} in the 7- and 13-element cores and suggests that the standard homogenization model is not appropriate for these small and highly heterogeneous assemblies.

Coolant Void Coefficient

The change in reactivity due to loss of coolant from the central channel of the 13-element core with 4.64 wppm ^{10}B in the moderator was calculated using the HAMMER code. The

calculated and experimental values are shown in Table 3.1. Calculated values are higher than experiment and lie outside the experimental uncertainties. There is a considerably higher discrepancy when H_2O coolant is used.

TABLE 3.1. Reactivity Change Due to Loss of Coolant from Central Channel in PRCF Experiments

^{10}B in D_2O, wppm	D_2O Coolant		H_2O Coolant	
	Experimental	Calculated	Experimental	Calculated
4.64	-0.65 ± 0.1 mk	-0.8936 mk	-3.8 mk	-6.61 mk

PRTR Critical Experiments

The analytical correlation of the PRCF critical experiments yields useful information regarding potential problems in the analytical correlation of the experiments conducted in the PRTR. In applying the same theoretical methods to the analysis of the PRCF and the PRTR experiments certain trends in correlation results are expected. The observation of these trends helps to identify limitations in the methods.

Effective Multiplication Factor, k_{eff}

The k_{eff} values were calculated for two of the initial critical experiments conducted in the PRTR. These experiments were the 55-element core with 21.00 wppm ^{10}B in the moderator and 31-element core with 12.4 wppm ^{10}B in moderator, which contains 99.4% D_2O and 0.6% H_2O. The coolants used in these experiments contained 97% D_2O and 3% H_2O. The calculational methods[11] were the same as used in the PRCF analysis and were performed using the HAMMER, HTH, and 2DB computer codes. The calculated values of k_{eff} are compared with experimental values in Table 3.2. The results obtained using HTH and 2DB are in good agreement with experiment for the 55-element core. The discrepancy in the HAMMER result is -11 milli-k for the 55-element core. In the PRCF analyses,[11]

TABLE 3.2. Comparison of Calculated and Measured Values of the Effective Multiplication Factor, k_{eff} for PRTR Experiments

Number of Elements	^{10}B Concentration, wppm	Calculated k_{eff} HAMMER (4 Groups)	HTH (6 Groups)	2DB (6 Groups)	Experimental k_{eff}
55	21.0	0.989	1.002	0.995	1.0
31	12.4	1.016			1.0

k_{eff} obtained with HTH, HAMMER, and EXTERMINATOR were higher than the measured value for the smaller cores (approximately 2%) but decreased with increasing core size. For the 55-element PRTR core k_{eff} is closer to the experiment for all cases corroborating the trend. This trend is due to the fact that a smaller fraction of the core cells lie at the core reflector interface as the core size increases.

Reactivity Worth of ^{10}B Addition

The reactivity worth of ^{10}B addition to the moderator of the 55-element core was calculated with HAMMER. The calculated and experimental values are compared in Table 3.3. There is excellent agreement between the calculated and experimental results as was the case in the PRCF analyses.[11]

TABLE 3.3. Reactivity Worth of Boron-10 Additions

Concentration of ^{10}B in 55-element Core	Coefficient of Reactivity, milli-k/wppm Measured	Calculated
20.95	-8.6	-8.52
20.85	-8.6	-8.554

Worth of a Peripheral Fuel Element

The reactivity worth of a peripheral fuel element addition to the 31-element core with 12.4 wppm ^{10}B in the moderator and to the 55-element core with 21.0 wppm ^{10}B in the moderator was calculated with HAMMER. A fuel cell was homogenized and added as an annulus to the basic cylindrical core. The calculated

and the experimental results are shown in Table 3.4. The calculated values are lower than the experiment and fall within experimental uncertainty for the 32-element core and outside the experimental error for the 56-element core.

TABLE 3.4. Worth of a Peripheral Fuel Element

Cluster Number	^{10}B in D_2O, wppm	Worth of a Cluster, milli-k	
		Measured	Calculated
32	12.4	4.0	3.61
56	21.0	2.0	0.389

Coolant Worth

The reactivity worth of coolant in all the channels (fuel and reflector) for the 31-element core with 12.4 wppm ^{10}B in moderator and the 55-element core with 21.0 wppm was calculated with HAMMER. The worth of coolant in the central channel only and in the fuel channels only was also calculated for the 55-element core. The calculated and experimental values are shown in Table 3.5. The calculated values are consistently much higher than the experimental values. Further investigations are being made to determine the causes of this discrepancy.

TABLE 3.5. Core Coolant Worth

Number of Fuel Elements	^{10}B Concentration in D_2O, wppm	Reactivity Change, milli-k		
		Experimental		Calculated Δk
		Dry	D_2O	
31	12.4	0.0 (100.40)[a]	20 (85.92)	52.637
55[b]	19.6	0.0 (91.56)	0.80 (91.10)	6.120
55	21.0	-	-	9.835
55[b]	21.0	-	-	6.039
55[c]	21.0	0.0 (98.40)	0.02 (96.35)	0.526

a. *Number in parentheses are experimental critical heights.*

b. *No coolant in fueled channel only, unfueled channels are filled with D_2O.*

c. *No coolant in the central fuel channel only. All other channels are filled with D_2O.*

References

1. J. W. Kutcher et al. Critical Experiments with Batch Core Fuel in the Plutonium Recycle Critical Facility, (to be published). See also: Trans. Am. Nucl. Soc., vol. 10, p. 448. 1967.

2. R. I. Smith et al. "Critical Experiments with the UO_2—2 wt% PuO_2 Batch Core in the PRTR," Trans. Am. Nucl. Soc., vol. 10, p. 185. 1967.

3. Unpublished Data. Pacific Northwest Laboratory, Richland, Washington. (Preliminary Report)

4. J. E. Suich and H. C. Honeck. The HAMMER System: Heterogeneous Analysis by Multigroup Methods of Exponentials and Reactors, DP-1064. E. I. du Pont de Nemours & Co., Wilmington, Delaware, 1967.

5. J. R. Lilley, Computer Code HFN - Multigroup, Multiregion Neutron Diffusion Theory in One Space Dimensions, HW-71545. Available from Clearinghouse for Federal Scientific and Technical Information, Springfield, Virginia, 1961.

6. T. B. Fowler et al. EXTERMINATOR-2: A Fortran IV Code for Solving Multigroup Neutron Diffusion Equations in Two Dimensions, ORNL-4078. Oak Ridge National Laboratory, Oak Ridge, Tennessee, 1967.

7. W. W. Little, Jr. and R. W. Hardie. 2DB-A Two-Dimensional Diffusion-Burnup Code for Fast Reactor Analysis, BNWL-640. Pacific Northwest Laboratory, Richland, Washington, January 1968.

8. W. W. Little, Jr. and R. W. Hardie. 2DB User's Manual, BNWL-831. Pacific Northwest Laboratory, Richland, Washington, July 1968.

9. R. W. Hardie and W. W. Little, Jr. PERT-N, A Two-Dimensional Perturbation Code in Fortran-IV, BNWL-409. Pacific Northwest Laboratory, Richland, Washington, April 1967.

10. N. E. Carter and W. L. Purcell. Unpublished Data. Pacific Northwest Laboratory, Richland, Washington, 1969. (Preliminary Report: KINPAR: A Computer Code to Perform Perturbation Theory Calculation of Effective Delayed Neutron Fractions and Prompt Neutron Lifetime.)

11. *M. A. Mannan and D. L. Prezbindowski. "Theoretical Correlation of the PRTR Batch Core Experiment," Reactor Physics Technical Activities Quarterly Reports, April, May, June, 1968, BNWL-887; July, August, September, 1968, BNWL-921; October, November, December, 1968, BNWL-985. Pacific Northwest Laboratory, Richland, Washington.*

COMPARATIVE EXPONENTIAL MEASUREMENTS USING BF_3 AND INDIUM DETECTORS

J. H. Lauby and W. P. Stinson

In order to test the relaxation length measurement method in exponential assemblies, recent experiments in the Critical Approach Facility (CAF) included comparable flux measurements using indium foils (1/2 in. diameter, 0.007 in. thick) in addition to the usual measurements made using a BF_3 proportional counter (1/2 in. diameter, 4 in. long). Indium foils were used in four lattice spacings: one with UO_2–4 wt% PuO_2 fuel rods and three with Al–5 wt% Pu fuel rods. The Al–5 wt% Pu fuel rods are 1/2 in. diameter and 24 in. long, clad in 0.030 in. Zircaloy-2. The UO_2–4 wt% PuO_2 fuel rods are 1/2 in. diameter and 36 in. long, clad in 0.034 in. Zircaloy-2. The moderator and reflector were H_2O.

An indium foil is effectively a point flux detector while a BF_3 proportional counter integrates the flux over the length of the counter. If the flux is assumed to vary exponentially over the counter length, the ratio of the flux average ($\bar{y}$) to the flux at the center point (y_c) is given by;

$$\frac{\bar{y}}{y_c} = \frac{1}{2\lambda} \sinh 2\lambda \text{ (for a counter length of 4 inches)},$$

where λ is the exponential slope.

The expected difference for measurements made with point and integral detectors would not be a function of position but only a constant correction dependent on the counter length and exponential slope.

Both BF_3 and indium measurements were made in the central fuel rod position with the fuel rod removed. The aluminum tube containing the indium foils and 3/8 in. diameter polyethylene spacers was filled with water and polyethylene. The BF_3 traverse was made in an air-filled aluminum tube and included a varying amount of coaxial cable as a function of counter position.

With the Al–5 wt% Pu fuel, measurements were made using indium foils in the 0.85 in., 1.30 in., and 1.05 in. triangular pitch arrays. In the 1.05 in. lattice, relaxation lengths were measured as a function of boron concentration in the moderator for five nearly equal steps between 0 and 285 wppm natural boron. For the 229 wppm case, relaxation lengths were measured as a function of radius. The core sizes included 127-, 229-, and 240-rod arrays which contained 46, 83, and 87% of the critical mass respectively. Only the 127-rod core data could be analyzed as an exponential measurement. The axial flux shape in the two larger core loadings was no longer exponential.

With the UO_2–4 wt% PuO_2 fuel, indium measurements were made only in the 0.80 in. lattice. These measurements were also done as a function of core radius with loadings of approximately 50, 57, 69, and 81% of the critical mass.

Relaxation lengths were obtained by using program LEARN[1] to fit the equation

$$y = A \sinh B(C-x),$$

where y is the source-corrected counting rate, x is the position measured relative to the bottom of the fuel, A is a function of counting rate, B is the slope of an exponential without end effects, and C is the height above the bottom of the fuel

at which the extrapolated flux goes to zero. The positions measured with both detectors relative to the core for both types of fuel are shown in Figure 3.4. The relaxation lengths obtained with both types of detectors are listed in Table 3.6. About half of the values agree within their errors. For those that do not agree, the sign of the difference is about equally divided, implying that no systematic error is present. If the length of core traversed and the number of points measured with indium were equal to those measured with the BF_3 counter, the errors also would be more nearly equal in magnitude. The conclusions that can be drawn from these measurements are that the results are not significantly influenced by the method of measurement. The BF_3 detector, by virtue of a higher sensitivity, provides more usable data points to determine the relaxation lengths and axial extrapolation lengths with greater precision.

Indium foils were also used to measure the radial flux distributions in the 0.80 in. lattice with 277 rods of UO_2–4 wt% PuO_2 and in the 1.05 in. lattice with 229 rods of Al–5 wt% Pu fuel and 229 wppm boron in the moderator. The indium foils to be irradiated were attached to fuel rods on a diameter of the core. The data were fitted with a J_o Bessel function using program LEARN. The radial extrapolation lengths measured in each core agreed within their errors for irradiations made with the source in and with the source out of the exponential assembly. For the 0.80 in. and 1.05 in. lattices, the radial extrapolation lengths obtained were 7.4 ± 0.5 cm and 6.1 ± 0.2 cm respectively. Three values of the axial extrapolation length obtained from the hyperbolic sine fits to the BF_3 data agreed within their errors for the 0.80 in. lattice measurements. The error-weighted average value of these three measurements is 4.3 ± 2.3 cm, which is much smaller than the measured radial extrapolation length (7.4 ± 0.5 cm) obtained from the radial flux measurement.

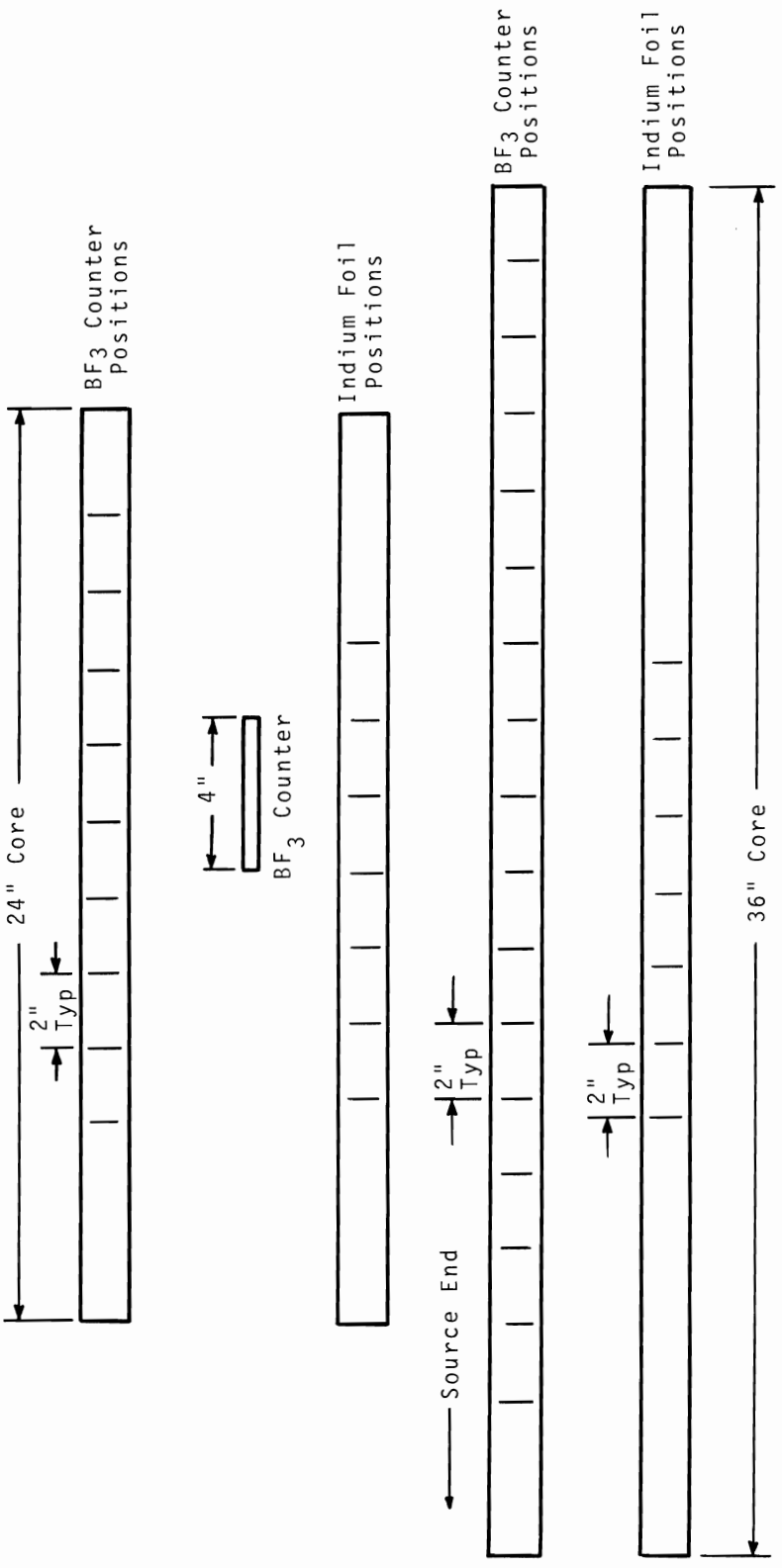

FIGURE 3.4. Relative Positions of the BF_3 Chamber and Indium Foils in the 24 in. Al–5 wt% Pu Core and in the 36 in. UO_2–4 wt% PuO_2 Core

TABLE 3.6. Relaxation Lengths and Extrapolation Lengths Measured Using Indium Foils and a BF_3 Chamber

Lattice Spacing, in.	Exponential Loading (No. of Rods)	Exponential Loading (% Critical)	Concentration, Natural Boron	Relaxation Lengths, cm: Indium Foils	Relaxation Lengths, cm: BF_3 Chamber	Extrapolation Lengths, cm: Axial (BF_3 Detector)		Extrapolation Lengths, cm: Radial (Indium)
			Al–5 wt% Pu Fuel					
1.05	85	51	0	17.6 ± 0.2	17.48 ± 0.05	6.6 ± 0.5		
1.05	91	49	48	16.4 ± 0.2	16.33 ± 0.03	7.1 ± 0.5		
1.05	109	52	101	18.1 ± 0.2	18.23 ± 0.07	7.9 ± 0.7		
1.05	121	52	164	19.8 ± 0.3	19.0 ± 0.03	7.4 ± 0.3		
1.05	127	46	229	17.9 ± 0.2	18.1 ± 0.4	7.9 ± 0.7		
1.05	229	83	229	-	-	-		6.1 ± 0.2
1.05	240	87	229	-	-	-		
1.05	151	52	285	20.5 ± 0.1	21.28 ± 0.02	8.1 ± 0.2		
1.30	109	51	0	20.7 ± 0.2	20.23 ± 0.06	4.1 ± 1.5		
0.85	109	49	0	17.6 ± 0.2	18.0 ± 0.1	6.8 ± 0.3		
			UO_2–4 wt% PuO_2					
0.80	169	50	0	17.5 ± 0.3	17.33 ± 0.07	4.6 ± 6.6	*	
0.80	193	57	0	20.8 ± 0.3	19.86 ± 0.08	3.8 ± 3.5	*	
0.80	235	69	0	27.3 ± 0.6	27.5 ± 0.4	7.4 ± 8.1	*	
0.80	277	81	0	50.3 ± 0.9	59.2 ± 1.3	21.2 ± 7.4		7.4 ± 0.5
						*4.3 ± 2.3 (average)		

Measured relaxation length are usually used to evaluate bucklings by equating the material and geometric buckling formulas and iterating on λ, the extrapolation length, which is assumed to be equal in the axial and radial directions. If the measured extrapolation length (λ_r), relaxation length (γ), and radius (R_e) for the 277 rod loading are substituted into the formula

$$B_m^2 = \left(\frac{2.405}{R_e + \lambda_r}\right)^2 - \left(\frac{1}{\gamma}\right)^2 \quad ,$$

a measured buckling value of 8.54 m^{-2} is obtained. Since the measured material buckling for a given fuel configuration is independent of the diameter of the exponential assembly used in the measurement, substitution of the other three measured values of relaxation length and related core radii into the buckling formula yields λ_r as a function of the radius of the exponential assembly. A plot of these results is shown in Figure 3.5. The

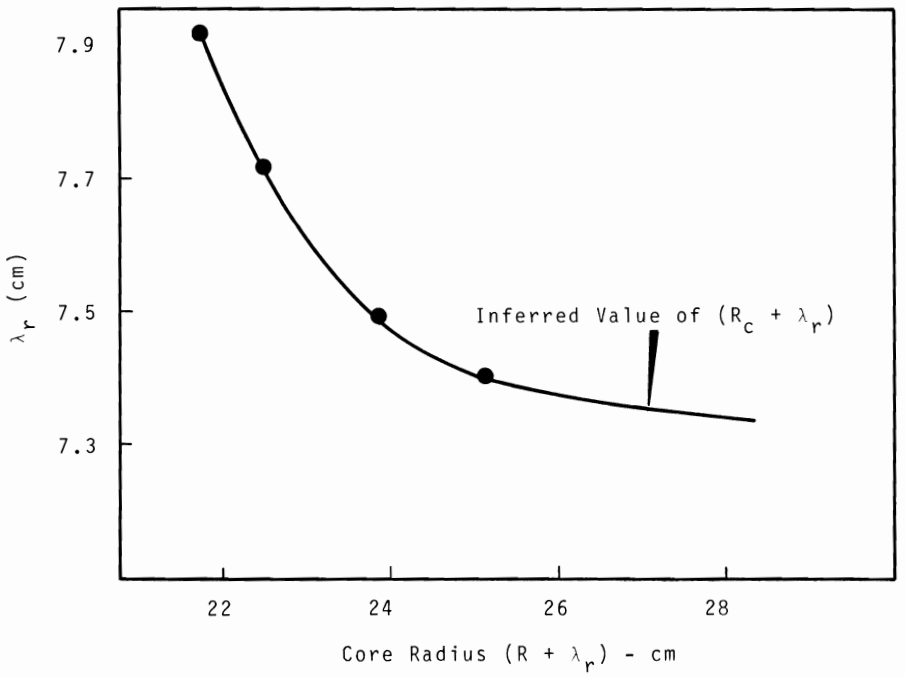

FIGURE 3.5. Variation of Radial Extrapolation Length with Core Radius for Rods of UO_2–4 wt% PuO_2 Fuel in Light Water Arranged in a 0.80 in. Triangular Pitch Lattice

calculated points have been fitted by inspection in order to extrapolate into the range of the critical radius for this core. Using the same buckling value and the measured value of the axial extrapolation length, $\lambda_a = 4.3 \pm 2.3$, in the geometric buckling formula

$$Bg^2 = \left(\frac{2.405}{R_c + \lambda_r}\right)^2 + \left(\frac{\pi}{H + 2\lambda_a}\right)^2 ,$$

one can solve for $(R_c + \lambda_r)$. R_c can be determined by reading λ_r from the curve in Figure 3.5 at $(R_c + \lambda_r)$ and subtracting. The number of fuel rods at critical obtained by this method is 342. The buckling and number of rods at critical for the 0.80 in. lattice are compatible with results reported previously for other UO_2–4 wt% PuO_2 lattices.(2)

References

1. *B. H. Duane. Maximum Likelihood Nonlinear Correlated Fields (BNW Program LIKELY), BNWL-390. Pacific Northwest Laboratory, Richland, Washington, September 1967.*

2. *W. P. Stinson and J. H. Lauby. "Approach to Critical Experiments with UO_2–4 wt% PuO_2-H_2O Lattices," Reactor Physics Quarterly Report, October, November, December 1968, BNWL-985. Pacific Northwest Laboratory, Richland, Washington, February 1969.*

REACTOR NOISE EXPERIMENTS IN THE PRCF WITH UO_2–2 WT% PuO_2 FUEL IN D_2O

J. H. Lauby

A series of reactor experiments with 19-rod clusters of UO_2–2 wt% PuO_2 fuel in D_2O(1) were performed in the Plutonium Recycle Critical Facility (PRCF) prior to loading that fuel into the Plutonium Recycle Test Reactor (PRTR) for the Batch Core Experiments.(2) Reactor noise techniques were used to measure reactor transfer function. The transfer function was measured for three core sizes and associated boron concentrations in the moderator.

Three BF_3 ion chambers (1.4 in. OD by 8 in. long) were spaced symmetrically at a radius of 33 in. around the axial midplane of the core. A block diagram of the recording circuit used is shown in Figure 3.6. Because the ion chambers were not of the guarded high voltage type, it was necessary to isolate the high voltage by feeding the signal through a capacitor-resistor network having the proper time constant. The signal was amplified and recorded on magnetic tape.

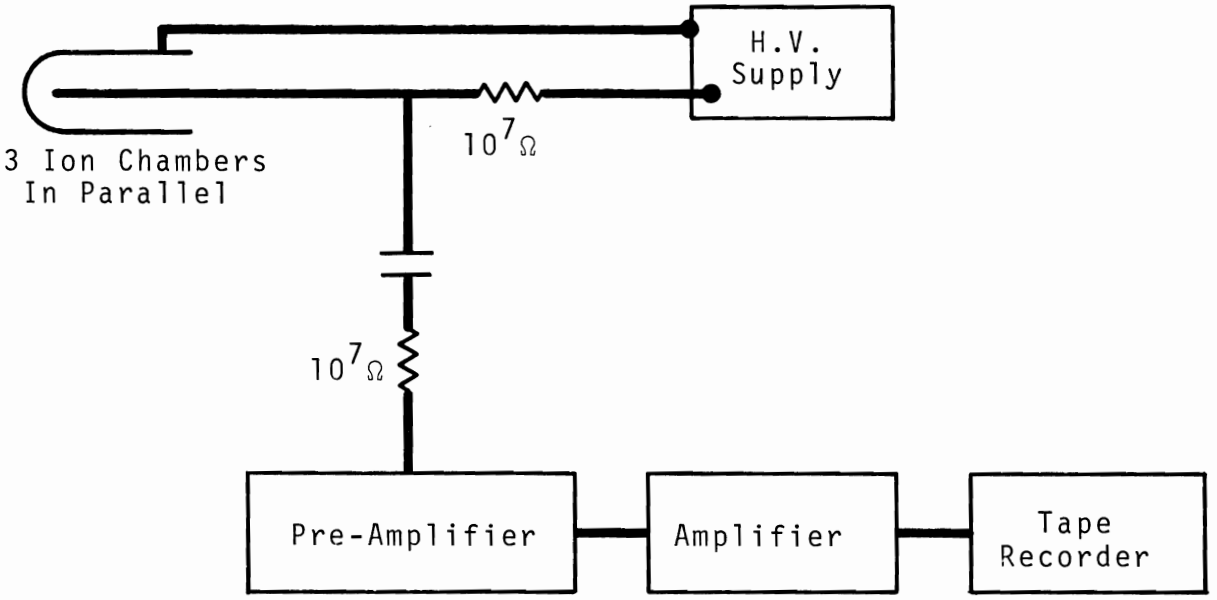

FIGURE 3.6. Block Diagram of the Instrumentation Used for Recording Reactor Noise

Analysis of the recorded noise was accomplished using a 10-channel frequency analyzer. Each frequency channel integrates the amplitudes over the length of the recording, and an analog-to-digital conversion gives numbers proportional to the sum of amplitudes for each frequency.[3] The recorded signals were analyzed at four tape speeds (1-7/8, 3-3/4, 7-1/2, and 15 in./sec), resulting in amplitudes measured at each of 40 frequencies. To obtain data at sufficiently low frequencies to define the transfer function for the 0.93 wppm case, the

original data tape was re-recorded to increase all frequencies by a factor of eight, thus providing amplitudes at 80 frequencies by a factor of eight, thus providing amplitudes at 80 frequencies to define the transfer function.

Each data set was fit with the equation,

$$|TF|^2 = A_1 + \frac{A_2^2}{\omega^2}\left(\frac{\omega^2 + A_3}{\omega^2 + A_4}\right) ,$$

where $|TF|^2$ is the square of the amplitude divided by the frequency, A_1 is the white noise background, A_2 characterizes the amplitude of the plateau of the function, $\sqrt{A_3}$ is 2π times the low frequency break, $\sqrt{A_4}$ is β/ℓ where β is the delayed neutron fraction and ℓ the prompt neutron lifetime, and ω is 2π times the frequency. Program LEARN[4] was used to fit the data. The values obtained for β/ℓ are listed in Table 3.7 along with values calculated using a multienergy group diffusion theory code, KINPAR.[6] The cause of the systematic discrepancies between experiment and calculation has not been determined.

TABLE 3.7. Comparison of Measured and Calculated Values of β/ℓ

Core Size (No. Clusters)	Moderator Boron Concentration, wppm ^{10}B	Measured β/ℓ	Calculated[5] β/ℓ
7	0.93	6.2 ± 0.3	4.42
13	4.70	9.8 ± 0.3	8.71
28	11.23	13.2 ± 0.4	12.38

The change in the ratio β/ℓ is related primarily to the decrease in the lifetime, ℓ, as the absorption cross section of the core increased, due to increased ^{10}B concentration in the moderator.

References

1. *J. W. Kutcher et al. "Critical Experiments with PuO_2-UO_2 Fuel and D_2O Moderator," Trans. Am. Nucl. Soc., vol. 9, p. 448. 1967.*

2. J. R. Worden et al. Physics Experiment - High Power Density Core of the PRTR, BNWL-221. Pacific Northwest Laboratory, Richland, Washington, 1966.

3. W. P. Stinson. Unpublished Data. Pacific Northwest Laboratory, Richland, Washinton. (Personal Communication)

4. B. H. Duane. Maximum Likelihood Nonlinear Correlated Fields (BNW Program LIKELY), BNWL-390. Pacific Northwest Laboratory, Richland, Washington, September 1967.

5. D. L. Prezbindowski and M. A. Mannan. "Theoretical Correlation of the PRTR Batch Core Experiment," Plutonium Utilization Program Technical Activities Quarterly Report, September, October, November, 1968, BNWL-963. Pacific Northwest Laboratory, January 1969.

6. N. E. Carter and W. L. Purcell. Unpublished Data. Pacific Northwest Laboratory, Richland, Washington, 1969. (Preliminary Report: KINPAR: A Computer Code to Perform Perturbation Theory Calculation of Effective Delayed Neutron Fractions and Prompt Neutron Lifetime)

A THREE DIMENSIONAL DIFFUSION THEORY MODEL OF THE MATERIALS TESTING REACTOR

C. M. Heeb and R. H. Holeman

In the course of designing a plutonium fueled core for the MTR, a model was developed for that reactor which must set some kind of a record for detail. The structural features of the reflector region of major neutronic importance are described discretely. This is accomplished in three dimensions with 28 by 18 by 39 mesh points and for two energy groups.

The MTR reflector is made largely of beryllium metal penetrated vertically by small cooling holes of variable spacing. This reflector surrounds the twelve major beam tube facilities which provide neutron egress from the core. Six of the beam tubes are in the horizontal plane through the core center and are splayed out at a nominal thirty degrees to each other. These are designated HB tubes. The other six tubes, seen from above, are DB or down beam tubes and fall along the same lines as the HB tubes, but in the vertical direction they interface the core above the HB tubes and are at an angle with respect to vertical. Aside from other small irradiation facilities, the other major structures are the horizontal through tube facility (HT1), which grazes the core just below the midplane at the west end, and a cavity on the east side called the D1 piece, which is associated with the spent fuel discharge system. In attempting to describe this system, the following approximations were made:

1. Two vertical planes of symmetry exist which bisect the core in the east-west and north-south directions creating a quarter core bounded with two reflecting planes.
2. The quarter choosen was the northwest quarter containing the HT1 facility and the L13 position which will contain a regulating rod for the plutonium core.

3. The thermal neutron absorbing portion of the shim rods was represented in two regions, one a cadmium aluminum composite and the other a central cavity containing water. Below the absorber portion the two regions were a pure aluminum structural wall region and a follower fuel region.

4. The circular horizontal beam tube HB1 and HB2 were made rectangular in cross section to preserve area and volume. The angular-placed HB1 was represented by three displaced rectangular parallelohedrons whose center lines tracked the path of the beam tube.

5. The DB1 and DB2 tubes were handled in a similar volume-preserving fashion.

6. The proposed regulating rod was represented as a single rectangular region.

7. Reflector aluminum pieces (A pieces) were represented discretely.

8. The end fittings and other plumbing above and below the core was represented by a metal and water smeared homogeneous region 40 cm thick. Beyond this, pure water was assumed.

9. The HT1, a square duct, is represented as is, including the aluminum skirt plates interfacing the core.

10. The core is a two zone representation. The power portion being represented by a smear of the fuel plate meat, the clad, and the water coolant. The other zone is a smear of box edges and interstitial water between boxes. All smearing operations naturally contain thermal flux adjustments to preserve reaction rates over the region.

Most of the approximations are justified by the experience gained in the analysis of the engineering mock-up critical experiment in the PRCF.

The computing details implementing this model are as follows:

1. The three-dimensional, two-group diffusion theory code WHIRLAWAY[1] is used as a start.
2. The code was expanded to include 146 region inputs from a previous limitation of 98. The space points were decreased to 19,660 from the 20,000 previously allowed.
3. The memory requirement of the present version is 55,268 which leaves only 27 unused locations of the total made available to the user by the EXEC II software system on the UNIVAC 1108.
4. The running time is 1.2 min per iteration. The number of iterations to convergence depends on the degree of over relaxation used and on the quality and availability of starting group fluxes. From a flat flux start and an over relaxation factor of 1.5, between 200 and 300 iterations can be expected for 0.5 millik eigenvalue convergence.

References

1. *T. B. Fowler and M. L. Tobias. WHIRLAWAY - A Three Dimensional, Two Dimensional, Two Group Neutron Diffusion Code for the IBM-7090 Computer, ORNL-3150. Oak Ridge National Laboratory. 1961.*

VARIATION OF k_{eff} DUE TO COMPOSITION UNCERTAINTIES IN CRITICAL ASSEMBLIES

C. M. Heeb

In the analysis of a critical experiment, the question of how well the composition of the subject assembly need be known often arises. It is almost equally often dismissed with vague observations about the same effects in numerator and denominator cancelling out. In the case of some critical approach experiments performed as part of the Phoenix fuel program,[1] this persistent question was answered in some detail using a

variance theorem from elementary statistics. Although the actual variation of k_{eff} was small in this case, the method used to determine this fact may be of general interest and applicability.

The experiments consisted of variations on a cylindrical array of cans filled with moderator and fuel discs. The discs were polyethylene, pure aluminum and 20% Pu-Al alloy. A large amount of data was available on the disc wall thickness and the fuel weight percent. The 95% confidence level on fuel disc thickness was 2.5%; on weight percent it was 2%. The effect of these uncertainties was calculated using a linear model for k_{eff} as a function of weight percent and disc thickness:

$$k_{eff} = A_0 + A_1X_1 + A_2X_2$$

X_1 = disc wall thickness

X_2 = weight percent Pu.

The values of the three $\underline{A}$ constants were determined by calculating k_{eff} at various values of X_1 and X_2. One-dimensional diffusion theory in four energy groups was used for the space calculation. Multigroup cross sections were computed using HRG[2] and THERMOS.[3]

The theorem from elementary statistics that the variation in a linear function is given by the sum of the variation in the linear arguments times the square of the linear form coefficient was used next:

$$\text{Var } [k_{eff}] = A_1^2 \text{ Var } [X_1] + A_2^2 \text{ Var } [X_2] \quad .$$

The variation in wall thickness was determined by sampling the mean of 240 discs in five samples chosen at random from the data population. The weight percent variation was determined

analogously. The final variation in k_{eff} was then given by

$$\text{Var}\,[k_{eff}] = (0.86853 \times 10^{-3})^2 \times 2.932 \times 10^{-2} + (3.56096 \times 10^{-3})^2 \times 2.0238 \times 10^{-2} = 2.787 \times 10^{-7}$$

$$\sqrt{\text{Var}\,[k_{eff}]} = 0.000528 \quad .$$

Thus the 95% CL variation in k_{eff} due to the variation in the mean disc thickness and the mean weight percent would be 2.95×0.000528 or about ±1.6 millik: Certainly well within the usual uncertainty expected from critical experiment analysis.

References

1. *C. M. Heeb. "The Analysis of Phoenix Fuel Critical Approach Experiments," Reactor Physics Department Technical Activities Quarterly Report, April, May, June, 1967, BNWL-534. Battelle-Northwest, Richland, Washington, August 1967.*

2. *HRG (Hanford Revised Gam) is a site revision of the Multigroup Slowing Down Code GAMI.*

3. *H. C. Honeck. THERMOS, A Thermalization Transport Theory Code for Reactor Lattice Calculations, BNL-3826. Brookhaven National Laboratory, Upton, Long Island, New York.*

SENSITIVITY OF Al-Pu SYSTEMS TO RECENT CHANGES IN HRG

U. P. Jenquin and G. L. Gelhaus

Calculations have been made for various Al-Pu fueled systems to determine the effects of recent changes[1,2] to the HRG code[3] and data tape. Results are presented for two Phoenix fueled systems [a HFIR[4] region and the MTR fuel used in the PRCF[5]] and for three lattices of Al–5 wt% Pu rods.[6]

The Phoenix fueled systems contain a high concentration of plutonium (20 to 40 wt% Pu), and the plutonium contains about 20% ^{240}Pu. Since the plutonium isotopic concentrations

are so high, the fraction of absorptions occurring in the non-thermal energy range is quite high. Therefore, changes in the HRG code and the HRG data tape affect the results for the Phoenix fueled systems more than for the lightly loaded rods. The reactivity effects for the various systems are summarized in Table 3.8.

TABLE 3.8. Physical Description of the System and Reactivity Effects of the Changes in HRG

Parameter	Description of System				
System	HFIR	MTR	Al-Pu Rods		
Plate or Rod Pitch, in.	0.10	0.20	0.85	1.05	1.30
Weight % Pu in the Fuel	43	20	5	5	5
% ^{240}Pu in the Plutonium	23	20	5	5	5
Change to Program or Data	**Percentage Change in Neutron Multiplication**				
"Wings" ^{240}Pu Cross Section Data	-8.7	-3.3			
Allocation to Multi-Fine Groups	-4.4	-1.0	-0.06	-0.01	0.00
1969 Data Tape	-0.7[a]	-0.3[a]	-1.20[b]	-1.10[b]	-0.79[b]
H_2O Upscatter	-1.3	-0.9	-0.26	-0.17	-0.12
Intermediate R.I. for Admix Scatterer	+2.6	+1.1	+0.05	+0.02	+0.02

a. *Relative to 1967 data*

b. *Relative to 1965 data*

The 1967 HRG cross section data used with the 1967 HRG code gives a calculated effective neutron multiplication of 1.026 for the just critical MTR fueled loading in the PRCF. This version of HRG allocates the entire 1 eV resonance to one fine group. Hence, the wings of the resonance are subject to the same amount of self-shielding as the peak of the resonance. For systems containing a large amount of ^{240}Pu, the net result

is a spectrum averaged ^{240}Pu cross section which is too small. The "wings" ^{240}Pu method is an allocation of the ^{240}Pu cross section which places a larger portion of the resonance integral in the adjacent energy groups in HRG. Approximately 10% of the infinitely dilute resonance integral is placed in the adjacent groups and allocated in a manner suggested by a GAM-II calculation. Since the data in these adjacent groups is not self-shielded using resonance parameters, the calculated spectrum average cross section is larger than the value calculated with the 1967 HRG data. Reactivity calculations using the "wings" ^{240}Pu cross section data for the PRCF critical experiment and earlier PCTR-Phoenix experiments are in good agreement with experimental results.

Using the "wings" ^{240}Pu cross section data for the HFIR system lowers k_∞ by 8.7%. The HFIR system is more heavily fueled than the MTR system. Thus, the spectrum average ^{240}Pu cross section is probably too large because the cross section data is not shielded sufficiently.

The first change to the 1969 version of the HRG program[1] was to allocate the resonance cross section to more than one fine group. This change is theoretically more sound than using the "wings" ^{240}Pu cross section data. Relative to the 1967 program and the 1967 data, this change decreases k_∞ by 4.4% for the HFIR fuel and 1.0% for the MTR fuel. The effect is much less than the "wings" ^{240}Pu effect. However, part of the ^{240}Pu cross section is allocated to energies below the nonthermal to thermal cutoff. Thus, part of the resonance cross section is omitted in the calculation of k_∞. If all of the resonance cross section were included in the calculation of k_∞, it is estimated that k_∞ would be 0.7% lower for the MTR system. For the lightly loaded rod systems, the effect of the allocation change is either very small or negligible.

The second HRG change[1] was to update the cross section data tape with the best cross sections available. Using the 1969 data rather than the 1967 data lowers k_∞ by less than 1% for the Phoenix fueled systems. Using the 1969 data rather than the 1965 data lowers k_{eff} by about 1% for the Al-Pu rods.

The third HRG change[1] is to include the upscattering effects of H_2O. The effect of the change is to decrease k_∞ by about 1% for the Phoenix systems and by a few millik for the rod systems.

The last change to the HRG code[2] is to use the intermediate resonance integral formulation for the admixed scatterers in the fuel. This change increases k_∞ 2.6% for the HFIR system and 1.1% for the MTR system. For the rod systems the effect is negligible.

The combined effect of the four changes is to decrease k_∞ by 1.1% for the MTR fuel. Thus, the calculated effective neutron multiplication for the PRCF critical experiment would be about 1.015, or 1 1/2% higher than the measured value.

Absolute values of the few group parameters showing the effects of the various changes are listed in Table 3.9 for the HFIR fuel and Table 3.10 for the MTR fuel.

References

1. *J. L. Carter. "The Allocation of Resonance Contributions to Fine Groups in HRG," (Elsewhere in this report).*

2. *J. L. Carter. Private communication.*

3. *J. L. Carter. "Computer Code Abstracts, Computer Code-HRG," Reactor Physics Department Technical Activities Quarterly Report, July, August, September, 1966, BNWL-340. Battelle-Northwest, Richland, Washington, October 15, 1966.*

4. *E. T. Binford, T. E. Cole, and E. H. Cramer. The High Flux Isotope Reactor, ORNL-3572 (Rev. 2). Oak Ridge National Laboratory, May 1968.*

TABLE 3.9. Results of HRG Calculations for a HFIR Plutonium System

	1967 Program		1969 Program			
	"Wings" Pu-240	1967 Data	1967 Data	1969 Data	H_2O Upscatter	Intermediate R.I.
Group 3 (2.38 to 0.683 eV)						
σa^{240}	927	438	697	732	735	597
Σ out	0.3487	0.3634	0.3644	0.3638	0.3374	0.3407
Σ a	0.2357	0.1269	0.1853	0.1932	0.1941	0.1634
$\nu\Sigma f$	0.0549	0.0575	0.0577	0.0576	0.0582	0.0589
ϕ	0.0894	0.1060	0.0950	0.0940	0.1005	0.1057
One Group (10 MeV to 0.683 eV)						
Excess ^{240}Pu resonance contribution	1100	1158	1152	1152	1152	914
ηf	1.1161	1.2956	1.1995	1.1836	1.1612	1.2138
p	0.4571	0.5240	0.4885	0.4855	0.4727	0.4918
Σ out	0.01302	0.01486	0.01389	0.01380	0.01342	0.01394
k_∞	1.398	1.524	1.460	1.450	1.431	1.469

TABLE 3.10. Results of HRG Calculations for the MTR-PRCF System

	1967 Program		1969 Program			
	"Wings" Pu-240	1967 Data	1967 Data	1969 Data	H_2O Upscatter	Intermediate R.I.
Group 3 (2.38 to 0.683 eV)						
σa^{240}	1617	1114	1275	1311	1321	1170
Σ out	0.4064	0.4100	0.4112	0.4111	0.3820	0.3833
Σ a	0.09317	0.06761	0.07583	0.07767	0.07837	0.07068
$\nu\Sigma f$	0.01812	0.01831	0.01838	0.01840	0.01868	0.01874
ϕ	0.1429	0.1492	0.1465	0.1461	0.1578	0.1600
One Group (10 MeV to 0.683 eV)						
Excess ^{240}Pu resonance contribution	1845	1948	1944	1944	1944	1702
ηf	0.8525	0.9742	0.9342	0.9201	0.8909	0.9279
p	0.7615	0.7899	0.7813	0.7801	0.7707	0.7803
Σ out	0.02182	0.02260	0.02237	0.02233	0.02199	0.02225
k_∞	1.514	1.564	1.549	1.545	1.531	1.547

5. *D. D. Lanning and G. J. Busselman. Phoenix Fuel Program Progress Report, BNWL-635. Battelle-Northwest, Richland, Washington, November 1967.*

6. *J. H. Lauby and W. P. Stinson. "CAF Measurements with Al-5 wt% Pu Fuel in H_2O Moderator," Reactor Physics Department Technical Activities Quarterly Report, April, May, June, 1968, BNWL-887. Battelle-Northwest, Richland, Washington, November 1968.*

4.0 FAST REACTORS

COMPARISON OF MELT-II WITH FORE II AND NUTIGER

A. E. Waltar and A. Padilla, Jr.

A comparison of MELT-II with two other coupled neutronics - heat transfer digital computer codes, FORE II and NUTIGER, was carried out to assess its accuracy both under steady-state and transient conditions. MELT-II is an improved version of MELT-I. It is intended for estimating gross core behavior during major fast reactor excursions. However, the region of investigation of this study was limited to below substantial fuel melting since FORE II and NUTIGER are fixed-geometry codes which cannot be used for core meltdown analysis. Moreover, the modifications to the portions of MELT-II which treat fuel collapse and sodium voiding have not yet been completed.

The case chosen for comparison was a 1040 liter core divided into three equal-volume radial channels and seven equal-volume axial nodes. The three fuel pins representing their respective radial core regions consisted of a 0.230 in. (0.584 cm) OD, a clad thickness of 0.014 in. (0.036 cm), and a fuel pellet OD of 0.195 in. (0.495 cm). Variable fuel thermal conductivity was used along with the assumption that the conductivity is constant for temperatures greater than 1800 °C. No sintering, fuel swelling, or central void formation was assumed to occur for the fuel.

Steady-State Axial Temperature Distribution

The steady-state axial temperature distributions of the fuel, clad, and coolant are compared in Figure 4.1 for the hottest (inner) radial channel with the exact solution. The coolant temperatures calculated by MELT-II, FORE II, and NUTIGER agree well with the exact solution.

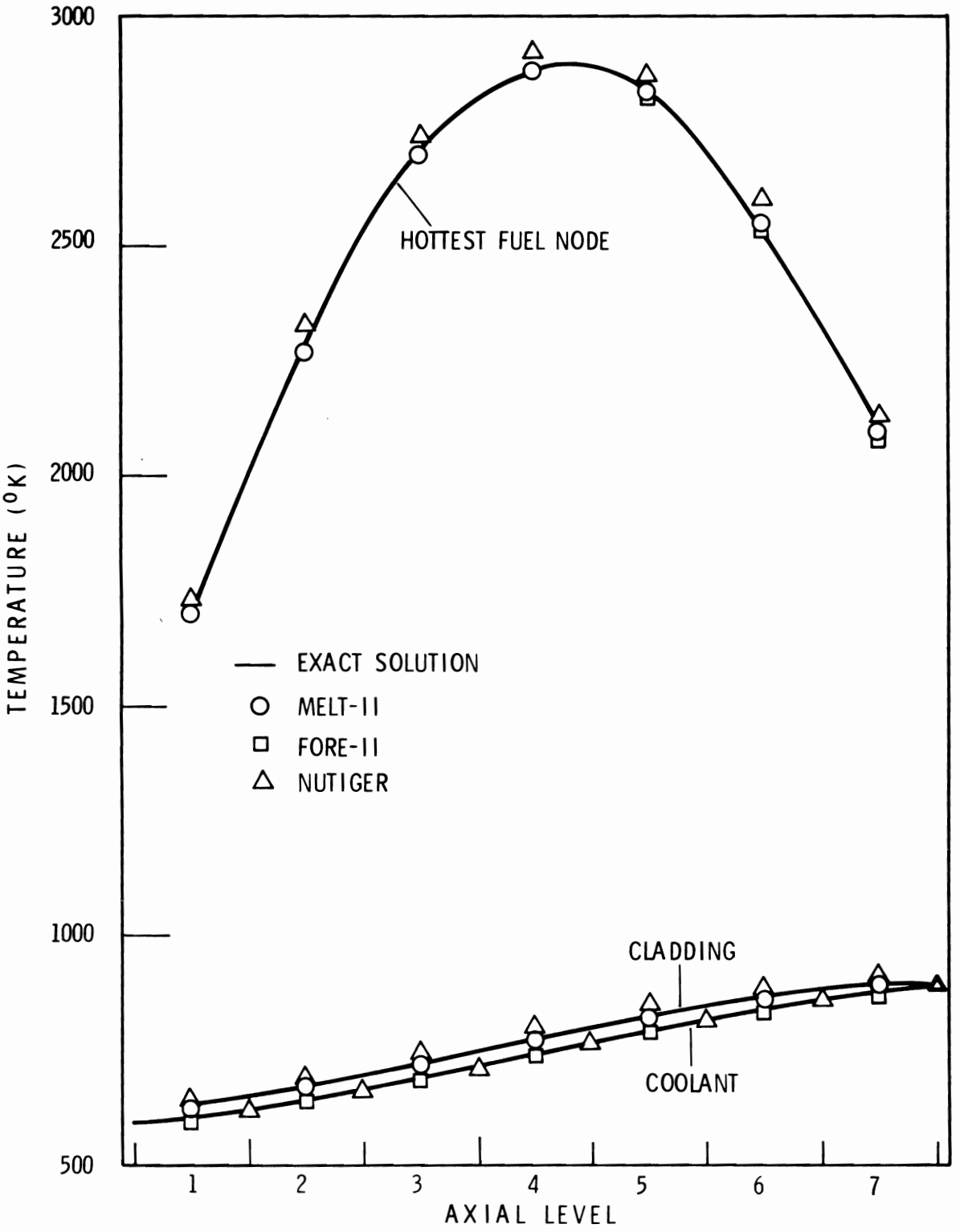

FIGURE 4.1. Comparison of Steady-State Axial Temperature Distribution

For this case, the centroid of the coolant nodes in MELT-II were assumed to be at the axial midpoint. MELT-II allows the centroid to be placed anywhere between the inlet and outlet of the node and for transient problems with low coolant flow rates the centroid should be placed near the outlet. However, the MELT-II output provides the coolant temperature at the outlet of the coolant node regardless of the location of the centroid. For FORE II the temperature of the coolant centroid is always taken as the arithmetic average of the inlet and outlet temperatures, but the coolant temperature, anywhere between the inlet and the outlet, assuming a linear temperature gradient, can be outputed. NUTIGER assumes that the centroid is always located at the outlet of the node.

The clad axial temperature distributions calculated by MELT-II and FORE II compare very well with the exact solution which assumes that the clad node should be connected to the average coolant temperature. Therefore, the NUTIGER clad temperatures are slightly higher because it assumes that the clad is connected to the coolant temperature at the outlet of the coolant node.

The fuel in each axial segment was subdivided radially into seven equally-spaced nodes, and the axial temperature distribution for the hottest (innermost) node is shown in Figure 4.1. MELT-II and FORE II agree quite well with the exact solution, but the NUTIGER temperatures are high due to the different connection between the clad and coolant. The effect has been aggravated because the fuel thermal conductivity decreases with temperature. That is, the slightly higher fuel temperatures at the outer edge of the fuel pellet results in slightly lower thermal conductivities which result in higher temperatures further in, etc.

Steady-State Radial Temperature Distribution

The steady-state radial temperature distributions at the axial midpoint of the hottest channel is shown in Figure 4.2. As already shown in Figure 4.1, the coolant and clad temperatures are identical for MELT-II and FORE II and slightly higher for NUTIGER because of the connection between the clad and the coolant. The fuel temperatures for both MELT-II and FORE II tend to be higher than the exact solution near the outer surface of the fuel pellet and then lower than the exact solution near the center. This is characteristic of the nodal approach which lumps all of the physical properties of the node into the centroid. Also shown in Figure 4.2 are the fuel temperatures calculated by a finite-difference analysis. The temperatures are very close to the exact solution. The finite-difference analysis will be used later for comparison of transient results for which there is no exact solution as a basis.

Transient Results

The effect of a 6$/sec reactivity ramp, without scram, on clad and fuel temperatures is shown in Figure 4.3 for the same axial level as in Figure 4.2. Although the clad temperatures for MELT-II and FORE II are initially identical, the slightly higher fuel temperatures in MELT-II causes its clad temperature to eventually rise faster than that of FORE II. The transient fuel temperatures for MELT-II, FORE II and NUTIGER have essentially the same shape and compare well with the results from the finite-difference analysis. Therefore, the difference in the time it takes to reach the melting point of the fuel is the result only of the different initial steady-state temperatures. For MELT-II, there is a slight (10 °K) rise in temperature as the fuel passes through melting because a variable specific heat model is used for the heat of fusion.

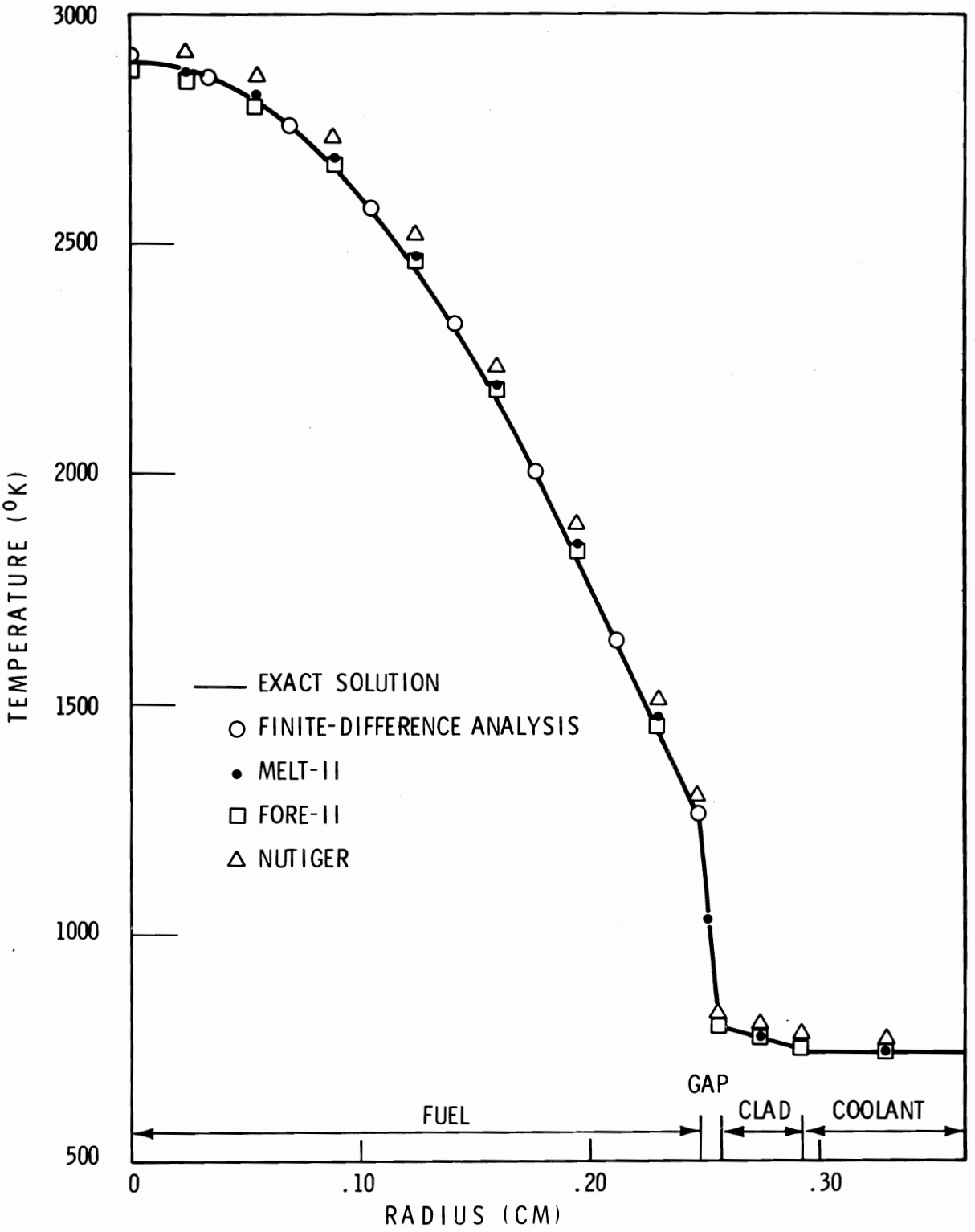

FIGURE 4.2. Comparison of Steady-State Radial Temperature Distributions

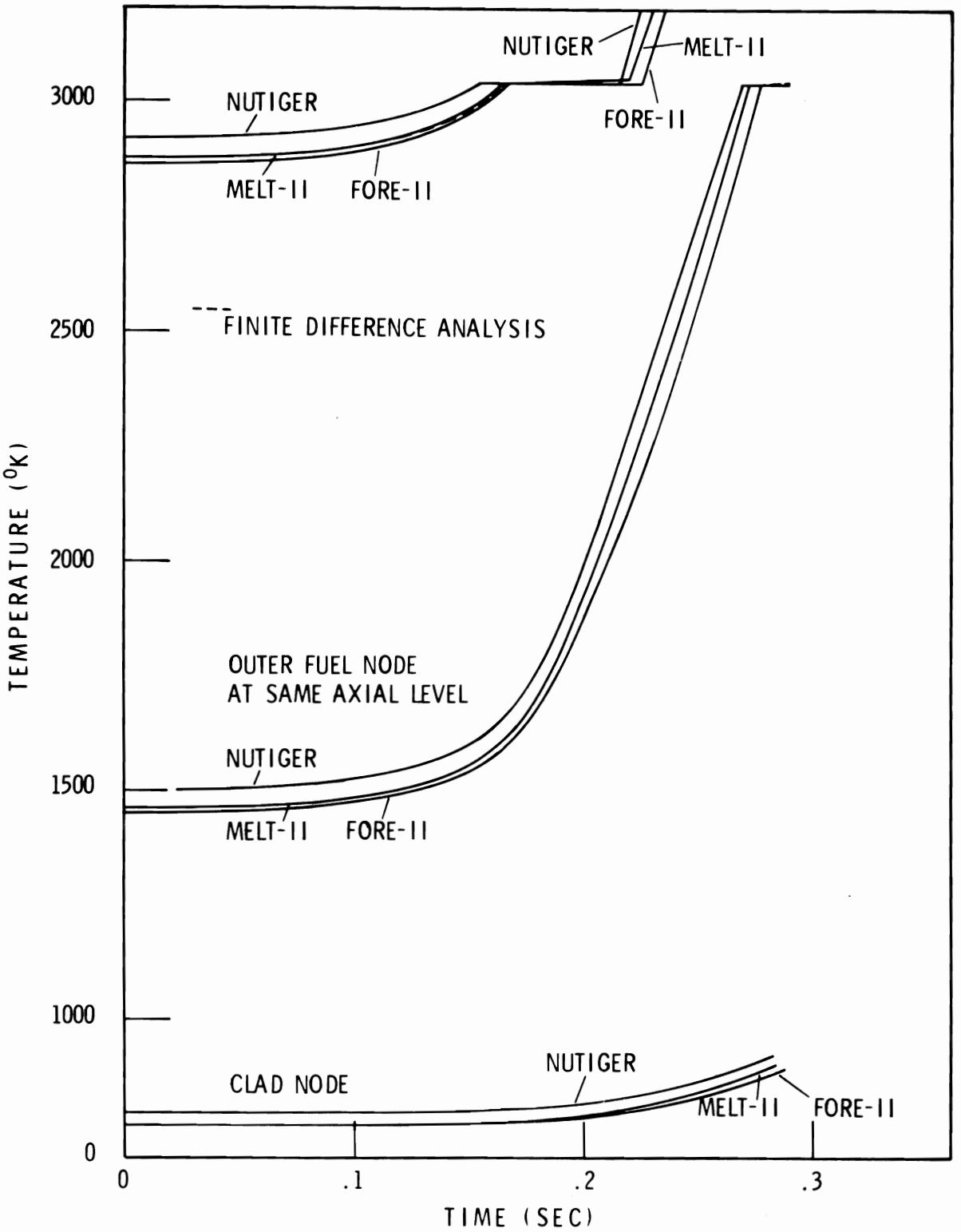

FIGURE 4.3. Comparison of Transient Temperatures for 6$/sec Reactivity Ramp Without Scram

A brief comparison of the UNIVAC 1108 computation time required by the three codes for the particular transient chosen is made in Table 4.1. The numbers given, however, are not completely revealing, since the codes use quite different methods for time step determination.

TABLE 4.1. Comparison of Running Time

Code	Comments	No. Time Steps	Total Run Time, sec (Including loading)
MELT-II	Finite lifetime (very tight error criteria)	416	82 ←
	Mixed mode (very tight error criteria)	92	59
FORE II	5% power change per time step	112	79 ←
	1% power change per time step	468	157
NUTIGER	∿4.5 msec time step (geometry determined)	65	126
	2 msec time step	145	240 ←

NOTE: *Arrows index the cases which are plotted*

NUTIGER and FORE II both require a geometric check on the largest permissible time step because they use explicit temperature calculation schemes. NUTIGER makes no other check and in order to insure accurate power calculations during super prompt critical conditions, the user must specify a short time step which is then held fixed throughout the transient. All reactivity feedback is one time step behind the power calculation. FORE II allows a variable time step which can be limited in size by the fractional power increase per time step. An extrapolation procedure is used to predict reactivity feedback effects in the new time step to enable reasonable power calculations to be made. No check is made, however, to determine whether the estimated feedback corresponds to that actually occurring due to the new temperatures.

MELT-II takes advantage of the exponential nature of the power variation in determining a variable time step (no geometric constraints are necessary because an implicit scheme is used for the temperature calculations). The time step is established once the power computed on the basis of an extrapolated feedback during the new time step agrees with the power computer with the actual feedback within a specified error criteria. This procedure allows very rapid feedback effects (e.g., core collapse or sodium flashing) to be adequately handled. The method works very well when the net reactivity is high and the power is changing rapidly, but is rather time consuming when the change in power is slow. To offset this difficulty, a zero neutron lifetime approximation was developed to perform the neutronics calculation for relatively slow portions of the transient. For "mixed mode" operation, the code selects the appropriate neutronics scheme to use.

From Table 4.1, it is noted that MELT-II and FORE II are comparable in running time, whereas NUTIGER is substantially longer, primarily because of the fixed time step procedure. The NUTIGER time step allowable from geometry considerations was not adequate for the neutronics calculations. Essentially, no difference in accuracy was detected for the two FORE II runs. The mixed mode approximation in MELT-II yielded a substantial savings in computer time over the rigorous method at the expense of a maximum error of only 12 °K in the peak fuel node and a 2% error in the power.

CRITICAL PARAMETERS FOR PuO_2-UO_2 SYSTEMS

C. L. Brown, L. C. Davenport, and C. A. Rogers

Studies were continued to establish minimum critical parameters for various forms of FFTF fuel for use in criticality safety analyses. Calculations completed are summarized below.

Homogeneous PuO_2-UO_2-Water Systems

Critical parameters have been calculated for water-moderated and water-reflected systems of 31 wt% PuO_2-U(Nat)O_2, with no ^{240}Pu and with 10 at.% ^{240}Pu, in the concentration range of 0.02 to 1.0 g Pu/cm^3 and into the undermoderated range of 1.0 g Pu/cm^3 to dry powder at theoretical density. A complete summary of results is given in Table 4.2. A unique characteristic of the 31 wt% PuO_2-U(Nat)O_2-H_2O system was identified this month. The volume and dimension curves versus plutonium concentration display a "triple point" of criticality, apparently due to the ^{238}U content. Thus, if a sphere of given diameter is chosen and the Pu concentration is gradually increased, criticality will be obtained. With further increase in concentration, the sphere will become supercritical, but as the concentration continues to increase the sphere will become subcritical. It will then remain subcritical through a region of increased concentration, finally becoming critical, and supercritical, once again. There are, thus, three concentrations within the sphere at which points the vessel becomes critical, with these points of criticality being separated by regions of concentrations in which the vessel is either subcritical (safe) or supercritical. This same phenomenon has been observed in Pu-H_2O systems containing high ^{240}Pu, but is not seen in the pure ^{239}Pu-H_2O system. For the latter system, as the concentration is increased, the critical volume continues to decrease.

PuO_2-UO_2 Fuel Pins in Air

The minimum critical number of 0.250 in. OD, 31 wt% PuO_2-U(Nat)O_2 fuel pins with 0.016 in. Type 304-SS clad and no ^{240}Pu was reported in our January 1969 Progress Report. If this is geometrically translated on the basis of conserving the critical mass of PuO_2-U(Nat)O_2 for the newer fuel core

TABLE 4.2. Calculated Critical Parameters for Homogeneous Water-Moderated, Water-Reflected, 31 wt% PuO_2-U(Nat)O_2 (ρ_o = 11.1 g/cm^3)

Plutonium Concentration, g/cm^3	Critical Parameters				
	Mass, kg Pu	Volume, ℓ	∞ Cylinder Diam, in.	∞ Slab Thick, in.	Areal Density, kg Pu/ft^2
No ^{240}Pu					
0.020 (HFN)	0.657	32.84	10.91	5.56	0.262
0.040 (HFN)	0.624	15.59	8.24	3.76	0.355
0.070 (HFN)	0.825	11.78	7.37	3.13	0.517
0.150 (HFN)	1.567	10.45	6.99	2.79	0.988
0.400 (HFN)	4.50	11.25	7.13	2.78	2.63
1.000 (HFN)	12.03	12.03	7.31	2.90	6.84
No ^{240}Pu					
1.00 (DTF)	11.11	11.11	--	--	--
3.05 (HFN)	29.75	9.76	--	--	--
3.05 (DTF)	25.79	8.46	6.45	2.51	18.08
10 wt% ^{240}Pu					
0.020 (HFN)	1.014	50.69	12.77	6.75	0.318
0.040 (HFN)	0.908	22.69	9.47	4.52	0.426
0.070 (HFN)	1.245	17.78	8.59	3.87	0.638
0.150 (HFN)	2.707	18.05	8.55	3.71	1.312
0.400 (HFN)	10.02	25.06	9.60	4.23	3.99
1.000 (HFN)	25.65	25.65	9.73	4.44	10.48
No wt% ^{240}Pu					
1.00 (DTF)	24.32	24.32	9.55	4.30	10.15
3.048 (HFN)	37.94	12.45	--	--	--
3.048 (DTF)	33.28	10.92	7.20	3.11	22.34

dimensions of 0.196 in. OD with clad having 0.230 in. OD and 0.200 in. ID, the number of pins for criticality is as follows:

Spacing Between Pins, in.	Number of Pins for Criticality
0.00	1899
0.04	2446
0.15	6742

PuO_2-UO_2 Pins in Water

Critical parameters were calculated for 24.5% PuO_2-U(Nat)O_2 fuel pins in water. The pin size and composition are described below:

	Actual	Used in Calculations
Enrichment, wt% PuO_2-UO_2	24.5 ± 0.05	24.5
Pin OD, in.	0.250	0.250
Fuel OD, in.	0.212	0.213
Clad	0.016-SS	0.016-SS
Density	93 ± 2 TD	95 TD
^{240}Pu, at.%	12 ± 1	11
^{235}U, at.%	-	0.711

Material bucklings were obtained using the Modified Hammer Code.[1] This code predicts reasonably accurately the material bucklings measured for 1.5 wt% PuO_2-UO_2 rods, and 6.6 wt% PuO_2-UO_2 rods. The results of the calculations are given in Table 4.3.

Subassemblies in Concrete - Dry and Water-Moderated

Calculations are in progress to determine the thickness of concrete necessary to reduce $k_{eff} < 0.95$ for a 14 × 14 square storage array of FFTF driver fuel bundles in concrete. This

TABLE 4.3. Calculated Critical Parameters for 24.5 wt% PuO_2-U(Nat)O_2 Pins in Water (250 in. OD; 0.016 in. SS Clad; 11 at.% ^{240}Pu)

Water to Fuel Volume Ratio	Critical Mass, kg fuel	Critical Volume, ℓ	Critical Slab Thickness, in.	Critical Cylinder Diameter, in.	Critical Areal Density, kg/ft^2
2.51	66.45	24.6	4.23	9.52	26.97
5.97	23.53	16.5	3.68	8.32	12.42
7.37	18.55	15.4	3.63	8.16	10.29
10.53	16.01	18.1	4.08	8.73	8.50
16.18	13.63	22.7	4.63	9.52	6.54
22.93	14.72	34.0	5.69	11.07	5.81
33.62	22.22	74.0	8.03	14.65	5.69
46.26	40.08	181.5	11.60	20.13	6.05

storage area is to be located in the FFTF Fuel Process Demonstration Facility, 308 Building. Tentative results indicate that 11 in. of concrete are needed. Evaluation is now in progress to determine if the amount of concrete needed will be reduced by the neutron absorption effect of the steel liner in each hole.

The fuel was 31 wt% PuO_2-U(Nat)O_2 at 90% of theoretical density, with no ^{240}Pu. The clad is 0.25 in. OD, 0.218 in. ID, Type 304 SS. The pin spacing within the fuel subassemblies was assumed to be 0.040 in. and the fuel length, 37 in. There were 217 fuel pins in a hexagonal array within a subassembly. The hexagonal subassemblies were 4.220 in. across flats with no retainers. The concrete had a 5.00 in. ID hole. The concrete OD was varied to give a specific multiplication constant. The cell calculation used fully reflecting boundary conditions to simulate an infinite array of storage cells. For the two region calculations, everything inside 5.00 in. OD was homogenized. For the three region calculations, region one homogenized everything inside the 4.200 in. hexagon; region two was water or void out to 5.00 in. OD; and region three was concrete.

The calculations were performed in cylindrical geometry using three computer codes, see Table 4.4. The multigroup diffusion theory code HFN was used with 18 group cross sections from GAMTEC-II. The multigroup transport theory code DTF also used 18 group cross sections from GAMTEC-II. The former cross sections included a correction for linearly anisotropic scattering, and the latter included linear anisotropy. The multigroup diffusion theory code 1DX with 26 group isotropic cross sections was used by L. L. Maas.

TABLE 4.4. Calculated Spacing Versus k_{eff} for Dry and Water Moderated FFTF Fuel Pin Bundles in a Concrete Storage Array (Hole size: 5 in.) Center-to-Center Spacing, Inches

	Fuel Pin Bundles + Water in Concrete					Fuel Pin Bundles + Void in Concrete		
	3 Region		2 Region			3 Region	2 Region	
k_{eff}	HFN	DTF	HFN	DTF	1DX	DTF	DTF	1DX
1.00	11.78	11.14	13.66	12.95	14.68	10.90	10.88	12.86
0.95	12.42		14.52	13.81	15.60		11.33	13.38
0.90	13.17		15.61		16.76		11.81	13.95
0.85	14.10		17.18		∿18.33		12.33	∿14.57

References

1. *L. J. Agee. Hammer - A Hanford Version, DUN-4829. Douglas United Nuclear Corp., Richland, Washington, 1968.*

HIGHLIGHTS OF AN NPTF VERTICAL CORE CONCEPT

Q. L. Baird and H. C. F. Ripfel

In compliance with a recent RDT directive, work on NPTF is being deferred. A brief summary of the NPTF design, which has been suitably adapted to the vertical FTR, is given in the following sections.

Reactor

The vertical core reactor concept features a main support grid plate on pillars from which a shell is erected to surround the core and reflector. Axial support for the typical NPTF driver fuel modules is provided by means of rods extending upwards from the main grid plate. These rods are individually removable to free the space underneath the reactor for the insertion of FTR driver fuel tests as well as NPTR control and safety modules. Lateral support is on two levels: (1) NPTR driver fuel modules are socketed in the spacer plates of the support rods which are restrained by clamps; (2) At the top, triangular spacer bars connect the individual modules. This scheme should provide for position reproducibility of the order of 1 to 2 mils. Otherwise, the modules are separated by gaps of about 30 mils to provide cooling channels and clearance for ease of loading. The control and safety rod drive units have been arranged at the bottom of the reactor to clear the top loading surface. The NPTF driver fuel modules have straight hexagonal cans which contain the fuel pins and the interstitial sodium. The average material density and the fuel configuration approximates that of the FTR. About 25% (55 of the 217) of the pins are removable from thin, 8 mil wall, stainless steel exchange tubes. The control rod drive units feature a double spring loaded scram assist. The in-core section of the control rods is of the sodium follower type. Poison is contained in an accessible annular space. The tertiary safety rods, non-scrammable, have full scale fuel followers.

Instruments and Control

NPTR control and safety is based on the measurement of the neutron flux. Conventional neutron detectors can be used in view of the favorable neutron to gamma flux ratio. Data processing and display (not control) is provided by a computer

which is envisioned to have a 24 bit word length and a 16 K memory size. Reduction of preliminary test data, as well as programmed control of a very small reactivity worth auto-rod, are additional capabilities of the computer.

RADIATION DAMAGE FLUXES AT THE VESSEL, TUBESHEET, FLOW METER, AND THERMOCOUPLE LOCATIONS

E. T. Boulette

In the evaluation of any concept, radiation damage to structural components and sensing devices imposes strongly influential design limitations. Since radiation damage is a function of the neutron fluence, neutron flux distributions (radially and axially) are of interest in design evaluation.

In Figure 4.4 the total neutron flux distribution through a typical fuel assembly is illustrated. Four below-core shielding configurations were investigated. In all four configurations, all regions were identical except for the Shield (Zone I) region, whose material composition differed in each case. The four compositions and the resulting fluences at the tubesheet are indicated in Table 4.5.

TABLE 4.5. Incident Fluences at the Tubesheet

Shield	Composition, vol%	Total Fluence, nvt
A	20% SS - 43% Na - 37% B_4C	1.5×10^{20}
B	20% SS - 80% Na	4.0×10^{22}
C	100% Na	1.0×10^{23}
D	57% SS - 43% Na	7.5×10^{21}

The above tabulated fluences are based on an assumed service life of 20 years and an availability factor of 0.75. From these results one sees that the tubesheet location is highly dependent upon the shield composition and the tolerable fluence level at the tubesheet. Fluence limits at the tubesheet (assuming a tubesheet temperature of 900 °F) are tentatively

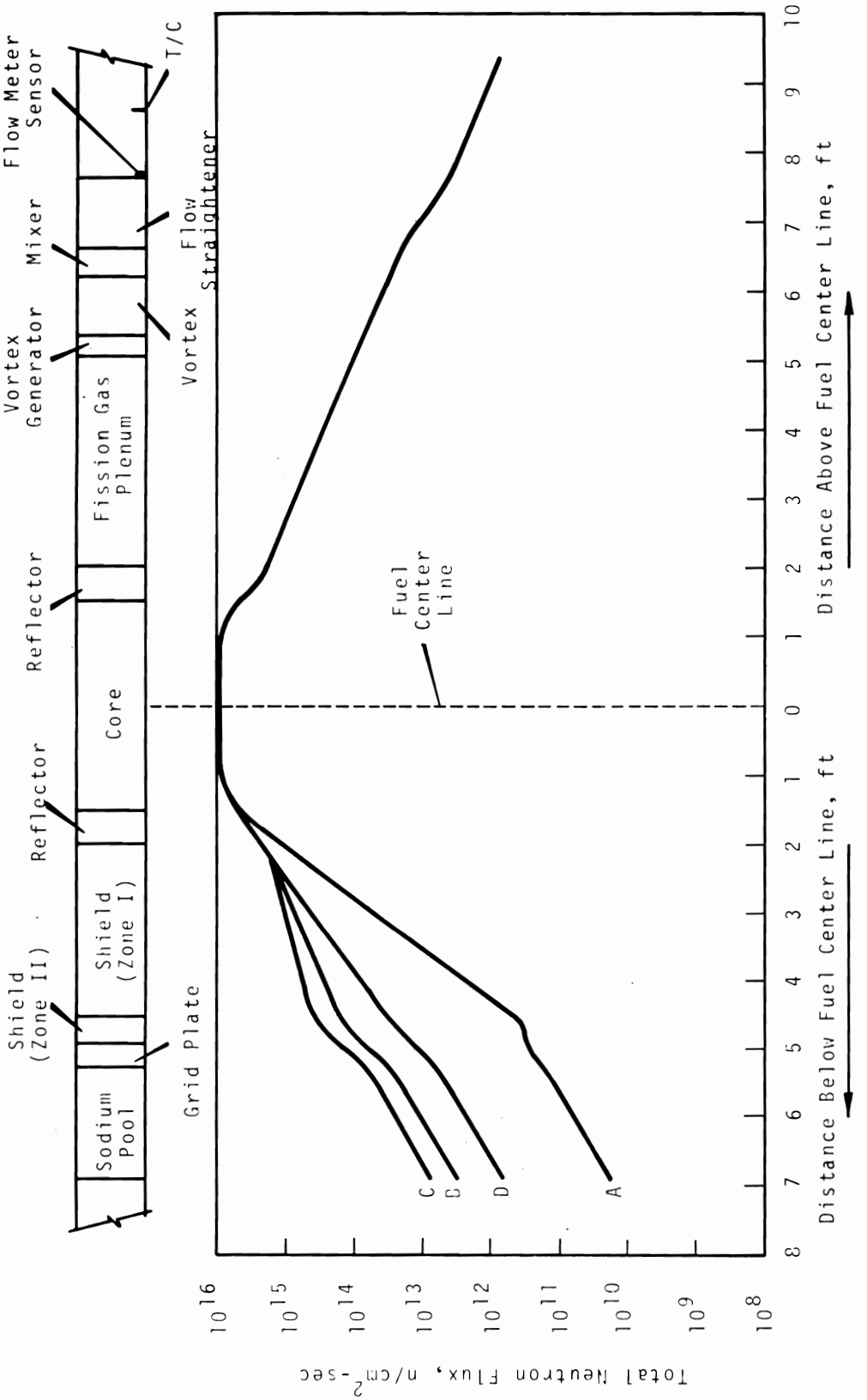

FIGURE 4.4. Axial Neutron Flux Distribution

established in the range 5×10^{21} to 2×10^{22} nvt. In Table 4.6 the tubesheet locations (in feet below the core) are listed for each shield that would satisfy a total fluence of 2×10^{21} nvt. Also tabulated are upper limits for localized fluences due to streaming. These upper limits are calculated by employing flux values at the listed tubesheet positions in Shield C, corresponding to 100% Na in Shield (Zone I). It should be emphasized that this technique of calculating localized fluences due to streaming is highly conservative.

TABLE 4.6. Tubesheet Locations and Localized Streaming Fluences for Shields, A, B, and D

Shield	Tubesheet Location, ft below the core	Streaming Fluence, nvt
A	2.0	4.0×10^{23}
B	4.5	1.2×10^{22}
D	3.5	6.0×10^{22}

Neutron radiation damage criteria are tentatively determined without consideration of the neutron energy spectrum. Because of this, shields yielding the same total number fluence will yield significantly different energy fluences.

In Table 4.7 are listed number and energy fluences at a fixed position below the core for Shields A, B, and D. Table 4.8 lists energy fluences and corresponding tubesheet locations in these same shields for a fixed nvt exposure. The importance of spectral consideration in defining radiation damage criteria is clearly indicated.

TABLE 4.7. Total Incident Fluences to Tubesheet Located 3.4 ft Below Core

Shield	Number Fluence, nvt	Energy Fluence, MeV/cm^2	Avg. Neutron Energy, MeV
A	7.5×10^{19}	1.3×10^{19}	0.17
B	2.0×10^{22}	5.8×10^{20}	0.029
D	3.8×10^{21}	1.4×10^{20}	0.037

TABLE 4.8. Tubesheet Locations and Energy Fluences for 2×10^{22} nvt Exposure Over a 2.5×10^{8} sec Lifetime

Shield	Location Below Core, ft	Energy Fluence, MeV/cm^2	Avg. Neutron Energy, MeV
A	0.9	2.2×10^{22}	1.1
B	3.4	5.8×10^{20}	0.029
D	2.0	1.1×10^{22}	0.55

Another design criterion of importance is the radiation damage to sensors, such as flow meters and thermocouples. Fluences have been calculated at the sensor locations indicated in Figure 4.4, and are tabulated in Table 4.9. The exposure time in this case is one year and the availability factor is 0.75.

TABLE 4.9. Incident Fluences at Sensor Locations

Sensor	Fluence, nvt ($E_n \gtrsim 0.1$ MeV)	Total Fluence, nvt
Flow Meter	2.5×10^{18}	1×10^{20}
Thermocouple	5.0×10^{17}	5×10^{19}

To meet a criterion of nvt ($E_n \gtrsim 0.1$ MeV) = 10^{21} nvt for one year exposure, the sensors could be located as close as 6 ft from the core center line, if streaming effects are ignored. Streaming through the fission gas plenum, however, will most certainly be of concern at this location. The locations indicated in Figure 4.4 will more than adequately satisfy the criterion of nvt ($E_n \gtrsim 0.1$ MeV) = 10^{21}.

The radial flux distribution is illustrated in Figure 4.5. The material composition of the shield is, in volume percent, 75% SS and 25% Na. If a 20 year service life and an availability factor of 0.75 are assumed, the total fluence at the vessel wall is 5×10^{21} nvt; at the core barrel, it is

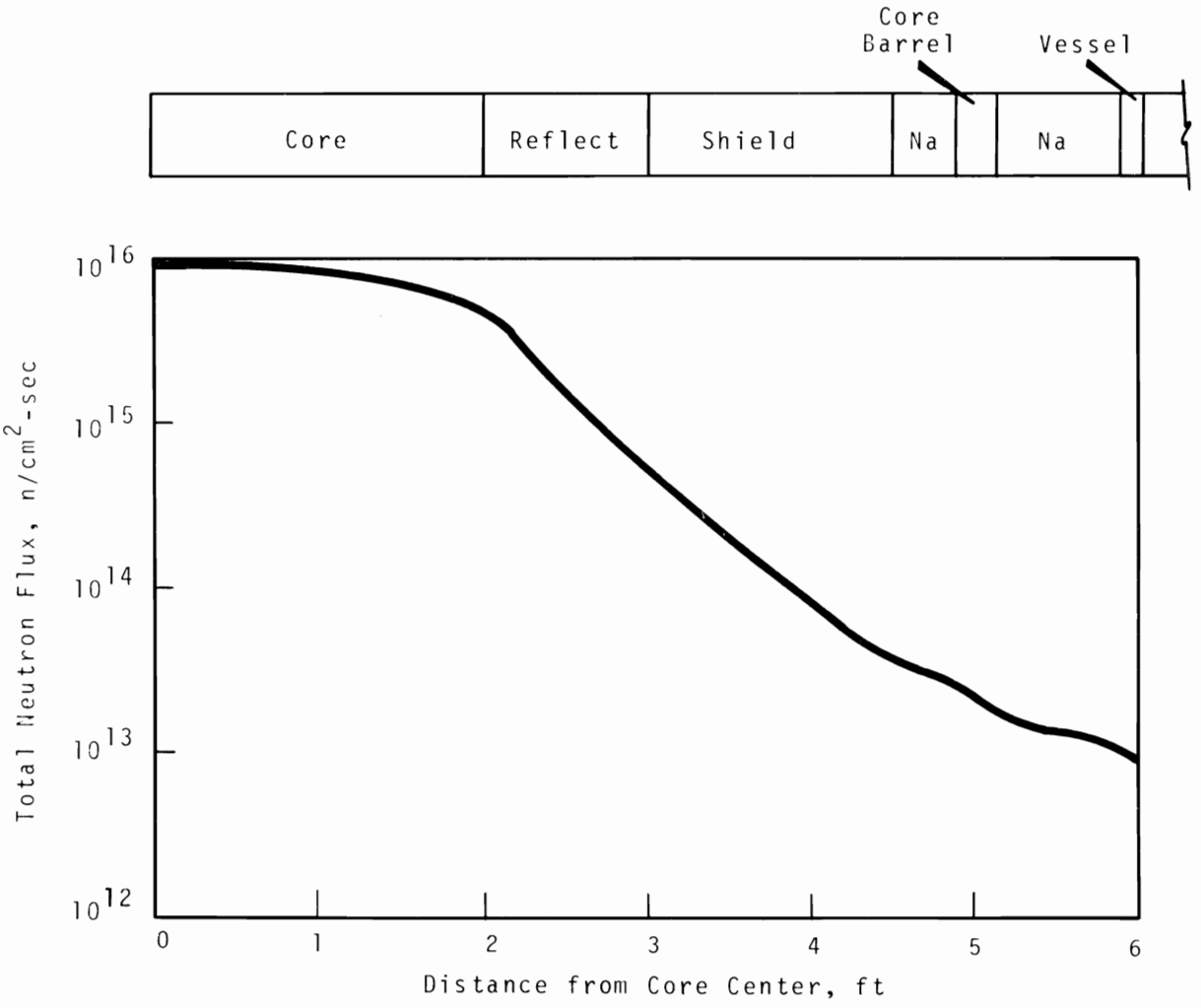

FIGURE 4.5. Radial Neutron Flux Distribution

1.3×10^{22} nvt. With steel temperatures of 900 °F, these total fluence values fall within the currently established tolerable fluence range.

All results are based on a reactor power level at 400 MW.

ESTIMATED UNCERTAINTY ASSOCIATED WITH DECAY HEAT CALCULATIONS

L. D. O'Dell

An estimate was made of the uncertainty in decay heat calculations introduced by the uncertainty associated with available nuclear data. Decay heat calculations are made using the computer code RIBD, which includes the contribution of each of 450 isotopes or isomeric states. The accuracy of the calculation is limited by the nuclear data. For this reason, the nuclear data library was recently updated to include the latest available information. The calculated decay heat rate associated with FTR fuel irradiated to goal exposure is shown in Figure 4.6 together with the estimated uncertainty in the value. Uncertainty in the fission product yields is based on Wolfsberg,[1] whereas the half life and decay energy uncertainties are based on Nuclear Data Sheet compilations. If the uncertainties in the nuclear data are assumed to be standard error, then the decay heat uncertainty limits represent the standard error in the calculated value.

References

1. *K. Wolfsberg. A Method for Estimating Fractional Yields from Low- and Medium-Energy Neutron Induced Fission, LA-3169. Los Alamos Scientific Laboratory, Los Alamos, New Mexico, January 1965.*

GAMMA INTENSITY NEAR CLOSED LOOP PIPES

C. A. Mansius

The sodium that is used as a coolant in FTR closed loop test facilities will become activated as it is circulated through the high neutron flux regions within the reactor vessel. Piping

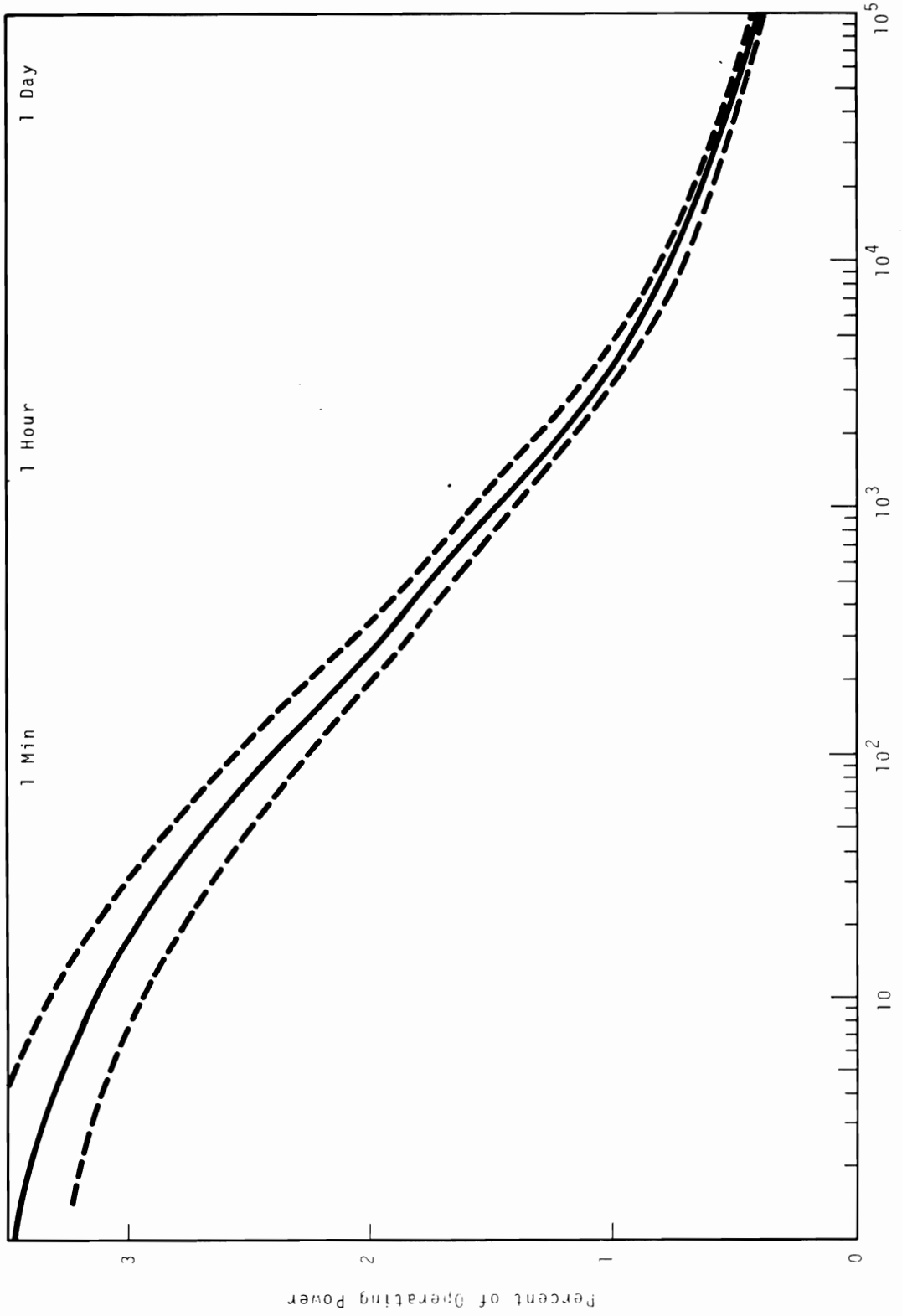

FIGURE 4.6. Estimated Uncertainty Associated with Decay Heat Calculations for FTR Fuel at Goal Exposure

carrying the radioactive sodium between the reactor and shielded test cells can, potentially, pass through regions in which personnel and/or equipment are to be located. We estimate the induced gamma activity in the test loop coolant to be about 0.01 Ci/cm^3 from ^{24}Na. However, the activity could be a factor of 2 or 3 greater or less depending upon the actual loop geometry. For 0.01 Ci ^{24}Na/cm^3, the gamma intensity at 1 ft in air from an 8 in. OD by 1/2 in. thick steel wall, infinitely long sodium filled pipe will be about 1700 R/hr. Approximately 1 in. of depleted uranium or 3-1/2 in. of iron are required to reduce the intensity by a factor of ten. The radiation intensity is proportional to the inside pipe area for smaller pipe sizes and will vary as 1/D, where D is the distance from the pipe surface in feet. These results can be used together with proposed criteria to establish piping shield requirements for specific conceptual arrangements.

An estimate of the 20 year gamma exposure at distances up to 10 ft from an 8 in. diameter sodium filled pipe was made to determine the shielding requirements to protect electrical equipment. The results at distances of 1, 5 and 10 ft for air, iron, and uranium shields are shown in Table 4.10. Assuming a useful lifetime of the order of 10^7 to 10^8 rads, about 2 to 4 in. of iron or equivalent shielding would be required to protect electrical equipment located in the vicinity of the closed loop piping.

TABLE 4.10. 20 Year Gamma Exposure, 8 in. Component Diameter, 0.01 Ci/cm^3 ^{24}Na

Distance from Component	Exposure, R			
	Air Shield	2 Inch Iron Shield	4 Inch Iron Shield	2 Inch Uranium Shield
1 ft	2.4×10^8	6.0×10^7	1.0×10^7	1.4×10^6
5 ft	4.9×10^7	1.3×10^7	3.2×10^6	3.8×10^5
10 ft	2.2×10^7	5.9×10^6	1.4×10^6	1.7×10^5

To perform maintenance work in the vicinity of the closed loop piping, shield requirements are minimized if the work can be delayed for several days to permit decay of ^{24}Na. For example, the radiation intensity from ^{24}Na at the surface of a 3 in. pipe shielded by 3 in. of iron is estimated to be about 10 mR/hr eight days after shutdown.

GAMMA INTENSITY NEAR FTR

C. A. Mansius

The gamma intensity following shut down of the FTR is of interest for locating neutron sensing elements for use in monitoring shutdown flux levels and reactivity status of the reactor. The computer code ISOSHLD was used to estimate the gamma intensity from the fission products in a right circular reactor 57.6 cm in radius and 91.4 cm high, with an average density of 5.055 g/cm^3. It was assumed the mixed oxide fuel had been irradiated to goal exposure at a power level of 400 MW. For these calculations it was assumed a sensor would be located 15 cm from the surface of the core, which corresponds to the midpoint of the second reflector ring. The first reflector row would provide a 10 cm thick shield composed of 75 vol% steel and 25 vol% sodium. Consideration was also given to the effect that could be achieved by use of additional tungsten shielding. Results are summarized in Table 4.11.

TABLE 4.11. Gamma Intensity in Middle Reflector Ring as a Function of Decay Time

Decay time, days	Gamma Intensity, R/hr	
	Base Case	5 cm of Tungsten
0	3.3×10^6	3.5×10^4
1	3.8×10^5	2.6×10^3
3	3.0×10^5	2.2×10^3
10	2.0×10^5	1.5×10^3
30	1.0×10^5	6.2×10^2

5.0 CRITICAL MASS PHYSICS

CRITICALITY OF HETEROGENEOUS PLUTONIUM-URANIUM MIXTURES

L. E. Hansen, S. R. Bierman and E. D. Clayton

Critical experiments have been performed on heterogeneous Pu-U systems with average core compositions typical of the materials that will be encountered in the processing and recovery of fast breeder reactor fuels. These heterogeneous criticality data will provide an interim check on the computational methods and cross section data being used in survey calculations on homogeneous PuO_2-UO_2 systems, pending the availability of clean, homogeneous experimental criticality data.

The experimental assemblies examined consisted of alternate (but not equal thickness) layers of PuO_2-polystyrene and depleted uranium (0.222 wt% ^{235}U). Two PuO_2 fuels were used. One had an H/Pu ratio of 15 and contained 2.2 wt% ^{240}Pu, and the other had an H/Pu ratio of 5 with 11.46 wt% ^{240}Pu. There was not, however, a sufficient amount of either PuO_2-polystyrene fuel to obtain an unreflected critical assembly when the depleted uranium layers were included in the system. It was, therefore, necessary to reflect two sides of the H/Pu = 15 systems (see Figure 5.1), and to use a fixed uranium-free base of H/Pu = 15 material, with dimensions of 30.9 × 30.9 × 15.4 cm, as a driver for the H/Pu = 5 fuel (see Figure 5.2).

The criticality data for the experimental assemblies examined are summarized in Table 5.1. Multiplication factors computed using the GEM-III Monte Carlo code are also given in Table 5.1 for each experimental assembly involved. The computed values of k_{eff} for the measured critical core configurations are quite good, and in most cases, the deviations from unity are within the statistical uncertainties of the calculations.

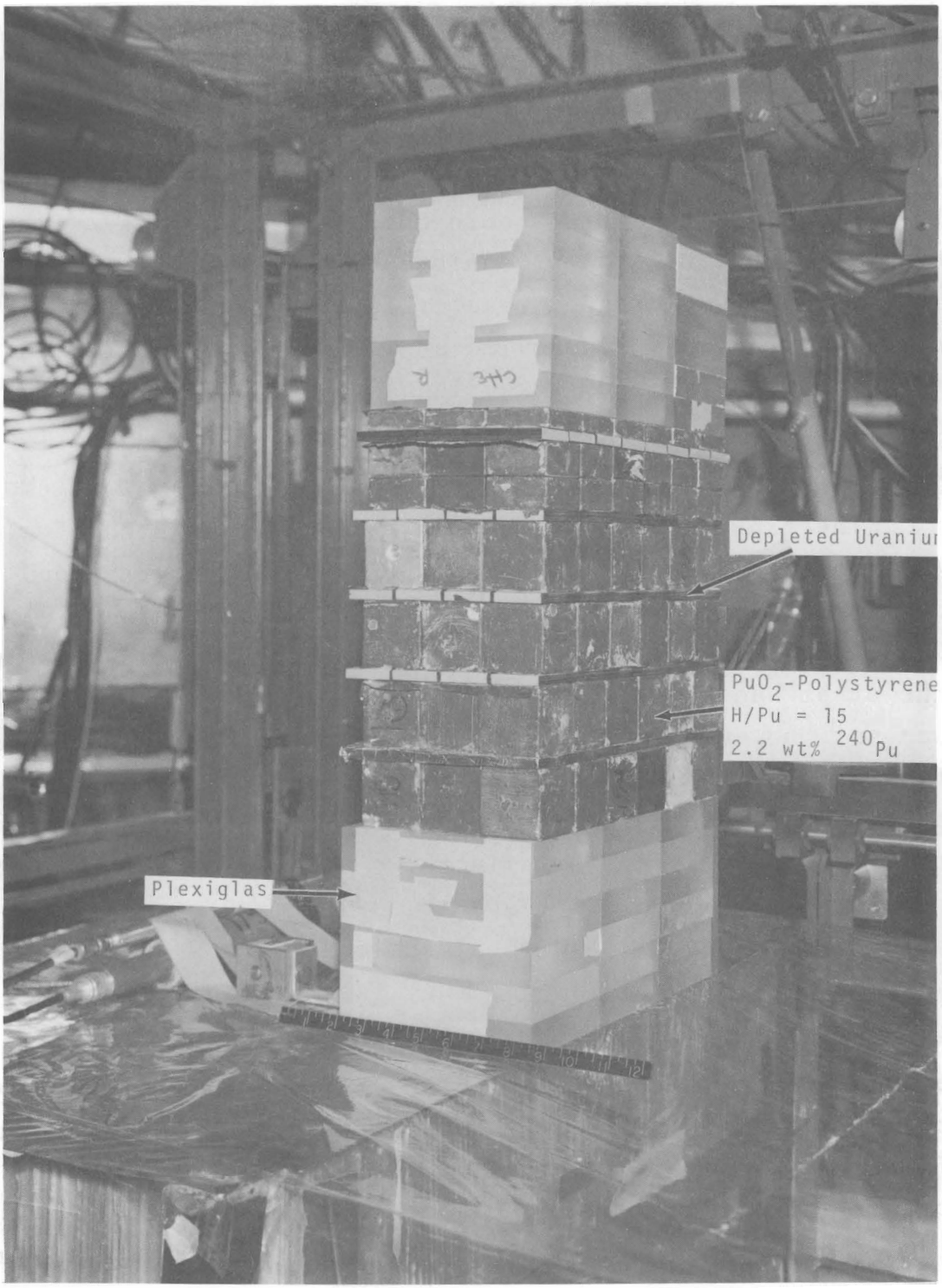

Neg 0690500-3

FIGURE 5.1. Experimental Assembly, H/Pu = 15

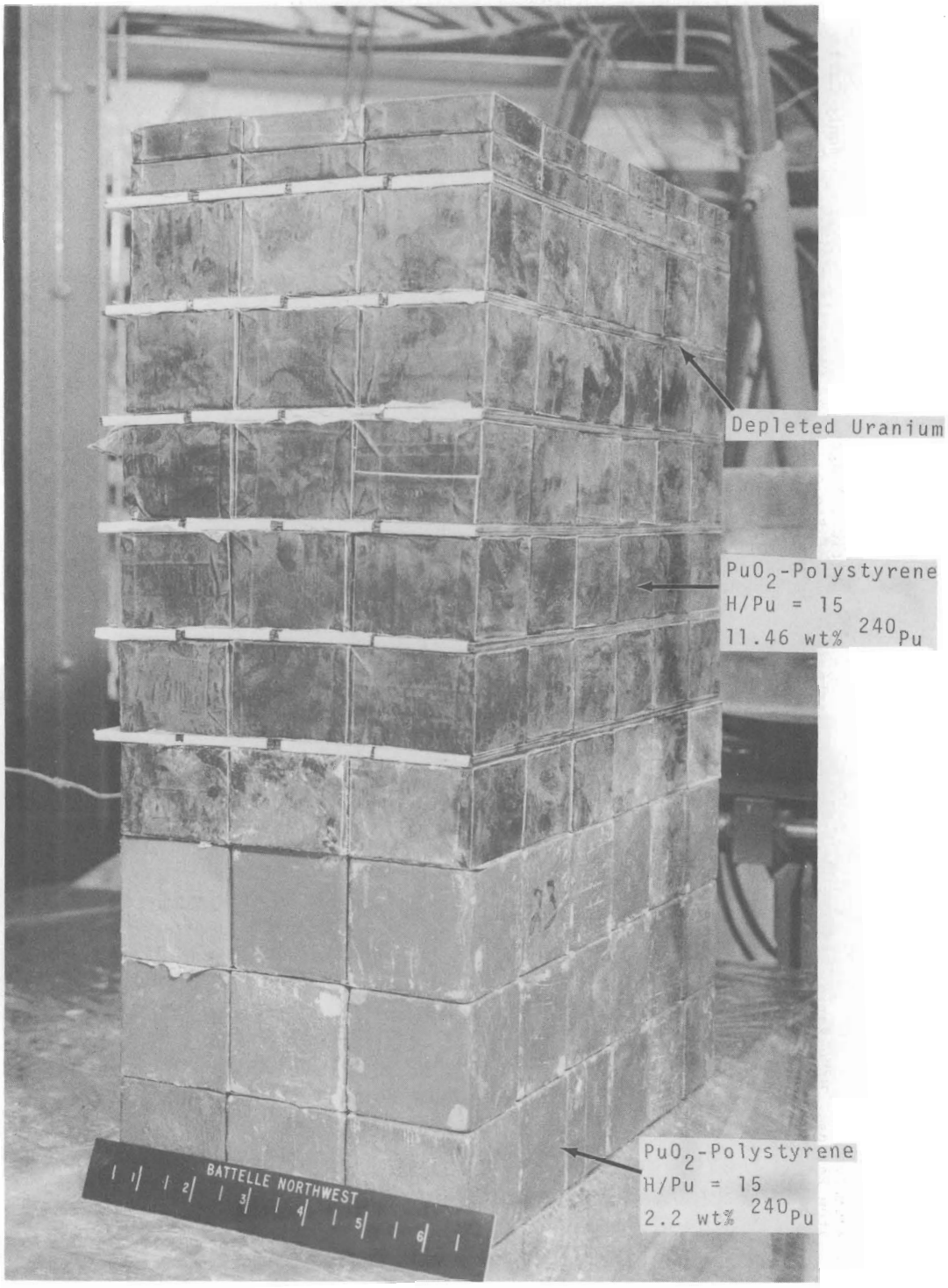

Neg 0691022-3

FIGURE 5.2. Experimental Assembly, H/Pu = 5

TABLE 5.1. Criticality of Heterogeneous Pu-U Mixtures

System Averaged Pu/Pu + U Atom Ratios for Region Containing Depleted U Layers	H/Pu Ratio for Region Containing U	Layers of Depleted U in Core	Nominal Thickness of U Layers, cm	Critical Length of Region Containing U Layers, cm	Critical Quantity of Pu in Region Containing U, kg	Monte Carlo Calculations of keff (GEM-III)
I - Two Region Rectangular Parallelepiped: Uranium-free region of PuO_2-polystyrene, 2.2 wt% ^{240}Pu, H/Pu = 15; Uranium-containing region of PuO_2-polystyrene, 11.46 wt% ^{240}Pu, H/Pu = 5; cross sectional dimensions 31.2 × 30.8 cm.						
1.0	5	0	0	23.30	49.68	1.0029 ± 0.0065
0.465	5	7	0.61	38.02	70.20	0.9923 ± 0.0047
0.554	5	6	0.46	33.66	64.48	0.9877 ± 0.0054
0.631	5	6	0.30	30.30	59.21	0.9926 ± 0.0051
0.748	5	5	0.20	28.31	57.02	0.9931 ± 0.0052
II - Single Region Rectangular Parallelepiped: Cross sectional dimensions of 30.9 × 30.9 cm; 6 in. Lucite reflector on top and bottom; PuO_2-polystyrene, 2.2 wt% ^{240}Pu, H/Pu = 15.						
1.0	15	0	0	22.79	23.92	0.9928 ± 0.0069
0.361	15	5	0.61	34.88	32.47	0.9956 ± 0.0060
0.462	15	4	0.46	30.53	29.61	0.9973 ± 0.0055
0.412	15	5	0.46	31.59	30.24	0.9957 ± 0.0056
0.553	15	4	0.30	28.64	28.37	0.9996 ± 0.0060
0.541	15	2	0.61	27.32	27.05	0.9961 ± 0.0062
0.700	15	4	0.15	26.35	26.76	0.9911 ± 0.0062

The paucity of experimental data and the need for further experiments is readily apparent when one notes that, apart from the experimental data reported herein at H/Pu ratios of 5 and 15, the only other data known to exist for comparable under-moderated Pu-U systems comes from the UKAEA (a single data point at an H/Pu ratio of 18.6 and with a Pu/U ratio of 0.335).

PULSED NEUTRON MEASUREMENTS ON ASSEMBLIES OF URANYL NITRATE

R. H. Chow and S. R. Bierman

In a series of PCTR experiments[1] to determine the minimum critical enrichment for hydrogenous uranyl nitrate, k_∞ measurements were made at different ^{235}U enrichments and over a range of H/U ratios in the region of optimum moderation. Fuel from the last set of k_∞ measurements was saved for use in developing the pulsed neutron source technique for determining the effective multiplication factor of in-plant subcritical multiplying systems. Also, since k_∞ was measured for this material, measured values of k_{eff} as a function of buckling resulted in an experimental determination of the neutron leakage as a function of buckling for this material.

Pulsed neutron measurements were made on assemblies of this uranyl nitrate material (2.26 wt% ^{235}U enriched and 11.2 atomic H/U ratio) having geometrical bucklings of 0.00967 cm^{-2} and 0.0137 cm^{-2}. Group constants from GAMTEC-II[2] were used with the measured decay constants to obtain values of k_{eff} from the following relationship:

$$k_{eff}\ (1 - \beta_{eff}) = 1 - \alpha_o \left[\nu \Sigma_a\ (1 + L^2\ B^2)\right]^{-1}$$

The prompt neutron decay constants were obtained from a five parameter, double exponential least squares fit which permitted a harmonic analysis of the pulsed neutron data to obtain the fundamental mode decay constant (α_o). These values of α

and the respective k_{eff} values are tabulated below along with k_{eff} values determined from the measured k_∞ value of 1.0294 for this composition uranyl nitrate and the following relationship:

$$k_{eff} = k_\infty (1 + M^2 B^2)^{-1}$$

B^2, cm^{-2}	α_o, sec^{-1}	Based on α_o	Based on k_∞	Percent Difference
0.00967	5787 ± 15	0.640 ± 0.01	0.632	-1.26
0.0137	7433 ± 23	0.547 ± 0.02	0.539	-1.48

The above measurements are supplementary to others currently being planned at the Critical Mass Laboratory for experimentally measuring k_{eff} of each of these two systems. Measured values of k_{eff} will permit the evaluation of the neutron leakage term employed in obtaining the above k_{eff} values.

References

1. *S. R. Bierman and G. M. Hess. Minimum Critical ^{235}U Enrichment of Homogeneous Hydrogenous Uranyl Nitrate, ORNL-CDC-5. Criticality Data Center Publication, Oak Ridge National Laboratory, June 1968.*
2. *L. L. Carter, C. R. Richey and C. E. Hughey. GAMTEC II: A Code for Generating Consistent Multigroup Constants Utilized in Diffusion and Transport Theory Calculations, BNWL-35. Battelle-Northwest, Richland, Washington.*

CRITICALITY OF $Pu(NO_3)_4$ SOLUTIONS IN SLAB GEOMETRY

R. C. Lloyd, S. R. Bierman, C. A. Rogers, and R. D. Johnson

The critical thicknesses of plutonium-bearing slabs are needed to provide an improved basis for nuclear safety guidance and criticality calculations. In the past, criticality data have been reported for slabs of $Pu(NO_3)_4$ solutions containing 4.6, 18.4, and 23.2 wt% ^{240}Pu.[1,2,3,4] These parameters were derived from experiments performed with the expandable-slab critical assembly which has been described previously.[5]

During the current reporting period, this assembly has been used to examine the criticality of $Pu(NO_3)_4$ solutions containing 18.4 wt% ^{240}Pu. Data were acquired for systems with a plutonium concentration of 66.5 g/liter in the bare configuration and reflected on both faces with either water or 1 in. of Lucite. The measured critical dimensions of the 42 in. wide vessel are listed in Table 5.2 with the results of a preliminary chemical analysis of the solutions.

TABLE 5.2. Criticality of $Pu(NO_3)_4$ Solution in Slab Geometry Slab Assembly - 42 in. Width, 18.4 wt% ^{240}Pu

Exp. No.	Reflector Status	Pu Conc., g/ℓ	Acid Molarity	Sp. Gr.	Total NO_3, g/ℓ	Critical Slab Thickness, in.	Critical Volume, ℓ	Critical Height, in.
491	Unreflected	66.5	2.4	1.1848	218.5	8.90	102.34	16.914
492	Unreflected					7.90	137.25	25.422
492R	Unreflected					7.90	138.11	25.578
493	Unreflected					7.90	137.92	25.595
494	Unreflected					7.60	171.09	32.861
495	Unreflected					7.50	189.81	36.911
496	Unreflected					8.90	101.84	16.832
497	Unreflected					8.40	113.22	19.779
498	1 in. Lucite on 2 Sides					8.40	81.39	14.292
499	1 in. Lucite on 2 Sides					7.90	85.21	15.881
500	1 in. Lucite on 2 Sides					7.40	92.05	18.275
501	1 in. Lucite on 2 Sides					6.90	106.14	22.538
502	1 in. Lucite on 2 Sides					6.40	145.72	33.234
503	1 in. Lucite on 2 Sides					6.30	161.54	37.392
504	Full Water					6.30	82.76	19.298
505	Full Water					6.90	72.36	15.447
506	Full Water					7.90	65.71	12.306
507	Full Water					5.90	98.24	24.373
508	Full Water					5.70	113.31	29.048
509	Full Water					5.60	124.75	32.521
510	Full Water					5.50	142.04	37.660

The results of a preliminary analysis of the data to obtain the best lateral extrapolation length and buckling for each system are given in Table 5.3. The extrapolation lengths were evaluated by minimizing the root-mean-square error in

the critical bucklings computed for each set of experiments. As a result, the critical buckling varies slightly with the different reflector materials. This variation is apparently due to the spatial dependence of the energy spectrum of the neutron flux within each system. Since this dependence is effective over most of the core thicknesses and is not the same for each system, the space- and spectrum-averaged material cross sections for each system are not identical. Thus, the material buckling of a given fuel may vary with the configuration of the critical assembly. This effect is being investigated.

TABLE 5.3. Bucklings and Extrapolation Lengths, 66.5 g/ℓ

Reflector	λ, cm	Buckling, m^{-2}
Water	λ sides = 6.49	151.4
1 in. Lucite	λ sides = 5.68	148.4
Unreflected	λ sides = 4.20	147.8

References

1. *R. C. Lloyd, E. D. Clayton and L. E. Hansen. "Criticality of Plutonium Nitrate Solutions in Slab Geometry," Trans. Am. Nucl. Soc., vol. 11, no. 1, p. 381. June 1968.*

2. *L. E. Hansen, R. C. Lloyd, C. A. Rogers and E. D. Clayton. "Criticality of $Pu(NO_3)_4$ Solutions in Slab Geometry," Reactor Physics Quarterly Report, July, August, September 1968, BNWL-921. Battelle-Northwest, Richland, Washington, November 1968.*

3. *R. C. Lloyd, E. D. Clayton and L. E. Hansen. "Basic Criticality Experiments with Plutonium Nitrate Solutions in Slab Geometry," Physics Research Quarterly Report, January, February, March 1967, BNWL-472. Battelle-Northwest Richland, Washington, May 1967.*

4. *R. C. Lloyd, S. R. Bierman, C. A. Rogers, and R. D. Johnson. "Criticality of $Pu(NO_3)_4$ Solutions in Slab Geometry," Reactor Physics Quarterly Report, October, November, December 1968, BNWL-985. Battelle-Northwest, Richland, Washington, February 1969.*

5. *R. C. Lloyd and E. D. Clayton. "Basic Criticality Experiments with Plutonium Nitrate Solutions in Slab Geometry," Physics Research Quarterly Report, July, August, September 1966, BNWL-340. Battelle-Northwest, Richland, Washington, November 1966.*

6.0 PUBLICATIONS AND PRESENTATIONS

PAPERS ACCEPTED FOR PRESENTATION

C. L. Brown. "Impact of Criticality on the Fabrication of Fast Reactor Fuel," invited for presentation at the Tenth Annual Meeting of the Institute of Nuclear Materials Management, Las Vegas, Nevada, April 28-30, 1969.

R. E. Schenter and R. L. Cassola. Theoretical Calculations of the Generalized Optical Potential for Neutron-^{16}O Scattering, BNWL-SA-2339-A. To be presented at the American Physical Society, Washington, D.C., April 28-May 1, 1969.

Papers for Presentation at the Fifteenth Annual Meeting of the American Nuclear Society, Seattle, Washington, June 15-19, 1969.

Invited Papers

D. D. Lanning and G. J. Busselman. Special Applications of Plutonium in Power Reactors, BNWL-SA-2353-A. Battelle-Northwest, Richland, Washington.

D. D. Lanning, A. D. Vaughn, M. D. Freshley (BNW); A. E. Aitken, D. L. Fischer, R. W. Friis (General Electric, San Jose); R. W. Miller (Phillips Petroleum, Idaho Falls); and M. A. Robkin (Univ. of Wash.). Nuclear and Fast Transient Aspects of Plutonium Particle Size in Thermal Recycle Fuel.

B. R. Leonard, Jr. Thermal Cross Sections of Plutonium Isotopes and the 1968-1969 IAEA Review.

R. C. Liikala, J. L. Carter, Jr., S. R. Dwivedi, G. L. Gelhaus, and V. O. Uotinen. Uncertainties in the Analysis of Plutonium Fueled Assemblies, BNWL-SA-2413-A. Battelle-Northwest, Richland, Washington.

Submitted Papers

D. E. Christensen and E. S. Murphy. Analysis of Nuclear Fuel by Gamma Scanning, BNWL-SA-2334-A. Battelle-Northwest, Richland, Washington.

R. P. Matsen, G. J. Busselman, R. H. Holeman, and R. C. Liikala. An Analysis of Uranium Fuel Irradiated in Yankee Reactor, BNWL-SA-2357-S. Battelle-Northwest, Richland, Washington.

PUBLICATIONS

S. R. Bierman, L. E. Hansen, R. C. Lloyd, and E. D. Clayton. "Critical Experiments with Homogeneous PuO_2-Polystyrene at 5 H/Pu," Nuclear Applications. January 1969.

C. L. Brown, L. E. Hansen and H. Toffer. "Material Buckling Measurements with 2.1 wt% ^{235}U Enriched Uranium Tubes in Light Water," Nucl. Sci. Eng., vol. 35, no. 3, p. 358. March 1969.

D. W. Glasgow, and D. G. Foster, Jr. "Effect of Nuclear Deformation on Fast Neutron Total Cross Sections," Phys. Rev. Letters, vol. 22, p. 139. 1969.

D. W. Glasgow and D. G. Foster, Jr. "Analysis of Fast Neutron Total Cross Sections for Effects of Nuclear Deformation," Bull. Am. Phys. Soc., vol. 14, p. 39. 1969.

R. P. Matsen. "Evaluation of Isotopic Dilution Method Used for Destructive Analysis of Irradiated Fuels," BNWL-CC-669. Battelle-Northwest, Richland, Washington, 1966. (Cleared for Offsite Distribution 3-10-69).

R. P. Matsen. EBWR Burnup Data, BNWL-978. Battelle-Northwest, Richland, Washington. (In publication)

E. S. Murphy, G. Manca, and D. E. Christensen. Nondestructive Analysis of Fuel Irradiated in the EBWR by Gamma Scanning, BNWL-1005. Battelle-Northwest, Richland, Washington. (In publication)

D. F. Newman and H. Mitsui. Highly Enriched U-Al, 0.95 wt% Enriched Uranium, and Li-Al Target Supercell - PCTR Experiments, BNWL-1029. Battelle-Northwest, Richland, Washington, March 1969.

R. E. Schenter, J. L. Baker, and R. B. Kidman. ETOX, A Code to Calculate Group Constants for Nuclear Reactor Calculations, BNWL-1002. Battelle-Northwest, Richland, Washington, March 1969.

H. S. Zwibel and A. G. Gibbs. Scattering of Long Ocean Waves, BNWL-913. Battelle-Northwest, Richland, Washington, January 1969.

DISTRIBUTION

No. of Copies

OFFSITE

2 AEC Chicago Patent Group
- G. H. Lee

15 AEC Division of Reactor Development and Technology
- Assistant Director for Civilian Reactors, DRD (1)
- Reactor Physics Branch, DRD, Chief (2)
- Division of International Affairs
- Chief Operations Branch
  - H. Werner
- Division of Production,
  - F. P. Baranowski (1)
- Division of Licensing and Regulations
  - C. D. Luke (1)
  - R. J. Odegaarden (1)
- Physics and Mathematics Programs,
  - G. A. Kolstad (1)
- Reactor Productions, Division of Production,
  - J. L. Schwennesen (1)
- Advanced Reactor Technology,
  - E. E. Sinclair (1)
- Water Reactor Branch, DRD (2)
  - D. E. Erb
- Gas Cooled Projects Branch (1)
- Core Design Branch (1)

218 AEC Division of Technical Information Extension

1 AEC Savannah River Operations Office
- R. Thorne

6 Argonne National Laboratory
- Reactor Physics Constants Center (4)
- R. Avery
- P. Gast

2 Atomic Energy of Canada Limited
- M. Duret
- C. Miller

No. of Copies

2 Atomics International
- H. Alter
- N. Ketzlach

3 Babcock and Wilcox Company
- H. Jones
- D. H. Roy
- W. A. Wittkopf

2 Bettis Laboratory, Westinghouse Electric Company
- D. Harris
- J. J. Taylor

3 Brookhaven National Laboratory
- J. Chernick
- H. Kouts
- S. Pearlstein

1 California Institute of Technology
- H. Lurie, Engineering Div.

10 CEN Saclay
Boite Postale 2
Gif-Sur-Yvette (S et O), France
- P. Lecorche
- G. Vendryes

1 CNEN - Casaccia
00060 - S. Maria Di Galeria
Rome, Italy
- Paolo Loizzo

2 CNEN-Centro Studi-Nucleaire
Casaccia, Rome, Italy
- Ugo Farinelli
- Augusto Gandini

1 Combustion Engineering, Nuclear Division
- R. Harding

No. of Copies	
2	Computer Sciences Corporation E. Z. Block R. J. Shields
2	Cornell University, Ithaca, N. Y. R. T. Cuykendall, Eng. Physics M. Nelkin
2	Assoc. C.E.N. Belgo Nucleaire 35 Rue Des Colonies, Belgium H. Bairiot L. Bindler
2	Duke University Durham, N.C. H. W. Newson, Physics Dept. W. J. Seeley, School of Eng.
6	E. I. du Pont de Nemours & Co., Inc., Savannah River Laboratory H. K. Clark J. L. Crandall G. Dessauer E. J. Hennelly H. Honeck J. Suick
10	EURATOM 53, Rue Billiard Brussels 4, Belgium A. de Stordeur
1	FFR - AB Afomenergi Studsvik, Pa NYKOPING Sweden Evelyn Sokolowski
4	General Atomic J. M. Neill L. W. Nordheim H. B. Stewart G. D. Trimble

No. of Copies

3 General Electric Company
Knolls Atomic Power Laboratory

R. Ehrlich
C. Lubitz
K. W. Seeman

3 General Electric Company
San Jose

D. L. Fischer
P. Greebler
S. Levy

1 General Electric Company
R and D Center
Schenectady, New York

W. R. Kanne

1 General Electric Company
Nucleonics Laboratory

H. W. Alter

2 Idaho Nuclear Inc.

R. G. Fluharty
E. Fast

1 Istanbul Technical University
Giimiis, suyer, Istanbul, Turkey

Director, Nuclear Energy Institute

1 Japan Atomic Energy Research Institute (JAERI)
Tokai-mura, Naka-gun, Ibarakiken, Japan

Hjime Sakata

1 Kansas State University
Manhattan, Kansas

W. R. Kimel, Nuclear Eng.

1 Kernforschungszentrum Karlsruhe
7500 Karlsruhe, Germany

Professor W. Haefele

No. of Copies	
1	Los Alamos Scientific Laboratory G. E. Hansen
1	Manhattan College Riverdale, New York, N.Y. Brother Gabriel Kane
2	Massachusetts Inst. of Technology Prof. Irving Kaplan T. J. Thompsom
1	North American Aviation Science Center E. R. Cohen
1	North Carolina State College R. L. Murray
1	Nuclear Materials and Equipment Corp. Apollo, Pennsylvania Karl Puechl
2	Oak Ridge National Laboratory F. C. Maienochien A. M. Perry
1	Pakistan Institute of Nuclear Science & Technology P.O. Nilore, Rawalpindi, Pakistan M. A. Mannan
1	Penn. State College W. F. Witzig
1	Phillips Petroleum Company Idaho Falls, Idaho W. B. Lewis
1	Power Reactor and Nuclear Fuel Development Corp. 9-13, 1-chome, Akasaka Minato-ku, Tokyo, Japan Setsuo Kobayashi

No. of Copies

1 Purdue University
P. N. Powers, Nucl. Eng. Dept.

1 Rensselaer Polytechnic Institute
E. R. Gaerttner

1 Union Carbide Corporation (ORNL)
E. B. Johnson

2 United Kingdom Atomic Energy Agency
Atomic Weapons Research Establishment
Aldermaston, Berkshire, UK
R. C. Lane (1)
Authority Health and Safety Branch,
Safeguards Division, Risley,
Warrington, UK
J. H. Chalmers (1)

1 United Kingdom Atomic Energy Authority
General Reactor Physics Division
Winfrith, England
C. G. Campbell

1 United Nuclear Corporation
White Plains, N.Y.
G. Sofer

1 University of Arizona
Tucson, Arizona
Monte V. Davis, Nucl, Eng. Dept.

1 University of Florida
Gainesville, Florida
R. E. Uhrig, Nucl. Eng.

1 University of Illinois
Urbana, Illinois
Frederick Seitz, Physics Dept.

1 University of Minnesota
Minneapolis, Minnesota
H. S. Isben, Chem. Eng. Dept.

No. of Copies	
1	University of Nevada Reno, Nevada T. V. Frazier, Physics Dept.
1	University of Notre Dame Notre Dame, Indiana E. W. Jerger, Dept. of Mech. Eng.
1	University of Oregon Eugene, Oregon J. L. Powell, Physics Dept.
2	University of Tennessee Knoxville, Tennessee A. H. Nielsen, Physics Dept. P. F. Pasqua, Nucl, Eng. Dept.
1	University of Toledo Toledo, Ohio J. J. Turin
2	University of Washington Seattle, Washington A. L. Babb, Dept. of Nucl. Eng. K. L. Garlid
1	University of Wisconsin Madison 6, Wisconsin M. W. Carbon, Nucl. Eng. Com.
1	U.S. Atomic Energy Commission DNR A Radkowsky
1	Virginia Polytechnic Institute Blacksburg, Virginia A. Robeson, Physics Dept.
1	Washington State University Pullman, Washington J. P. Spielman, Col. of Eng.

No. of Copies

3 Westinghouse Electric

C. A. Anderson
R. J. French
W. D. Leggett

ONSITE-HANFORD

1 AEC Chicago Patent Group

R. K. Sharp (Richland)

2 AEC RDT Site Representative

P. G. Holsted

9 AEC Richland Operations Office

M. J. Carrothers
J. T. Christy
C. D. Compton
W. Devine, Jr.
H. A. House
R. L. Plum
M. J. Rasmussen
C. L. Robinson
M. R. Schneller

8 Atlantic Richfield Hanford Company

S. J. Beard
M. H. Campbell
R. D. Carter
G. R. Kiel
R. J. Sloat
A. E. Smith
R. E. Tomlinson
ARHCO File

3 Battelle Memorial Institute

1 Donald W. Douglas Laboratories

J. Greenborg

No. of Copies	
10	Douglas United Nuclear
	T. W. Ambrose
	G. F. Bailey
	C. E. Bowers
	G. C. Fullmer
	L. L. Grumme
	R. O. Gumprecht
	J. H. Hamric
	R. H. Meichel
	R. Nilson
	DUN File
112	Battelle-Northwest
	F. W. Albaugh
	C. A. Bennett
	C. L. Bennett
	S. R. Bierman
	E. T. Boulette
	C. L. Brown
	W. L. Bunch
	S. H. Bush
	G. J. Busselman
	J. J. Cadwell
	J. L. Carter
	N. E. Carter
	D. E. Christensen
	R. G. Clark
	E. D. Clayton
	G. M. Dalen
	E. C. Davis
	F. G. Dawson
	D. R. de Halas
	R. F. Dickerson
	B. H. Duane
	J. B. Edgar
	G. W. R. Endres
	E. A. Eschbach
	E. A. Evans
	J. R. Fishbaugher
	D. G. Foster
	H. A. Fowler
	J. J. Fuquay
	G. L. Gelhaus
	A. G. Gibbs
	D. W. Glasgow
	V. W. Gustafson

Battelle-Northwest (contd)

C. E. Haines
R. J. Hall
L. E. Hansen
G. E. Hanson
O. K. Harling
H. Harty
C. M. Heeb
R. E. Heineman
H. L. Henry
R. J. Hoch
P. L. Hofmann
R. H. Holeman
U. P. Jenquin
R. D. Johnson
R. L. Junkins
G. J. Konzek
D. A. Kottwitz
J. W. Kutcher
C. R. Lagergren
D. D. Lanning
J. H. Lauby
B. R. Leonard, Jr.
D. L. Lessor
W. R. Lewis
R. C. Liikala
C. W. Lindenmeier
E. P. Lippincott
W. W. Little
R. C. Lloyd
R. P. Matsen
D. D. Matsumoto
G. C. Moore
D. F. Newman
R. E. Nightingale
T. J. Oakes
D. R. Oden, Jr.
H. M. Parker
R. S. Paul
R. E. Peterson
W. W. Porath
D. L. Prezbindowski
W. L. Purcell
W. A. Reardon
J. J. Regimbal
C. R. Richey
C. A. Rogers
W. C. Roesch
J. T. Russell
R. E. Schenter
L. C. Schmid (6)
G. L. Simmons
R. I. Smith
K. B. Stewart
W. P. Stinson
H. J. Svoboda, Jr.
D. H. Thomsen
C. R. Tipton, Jr.
V. O. Uotinen
A. D. Vaughn
E. E. Voiland
L. D. Williams
N. G. Wittenbrock
W. C. Wolkenhauer
J. R. Worden
D. C. Worlton
H. S. Zwibel
W. P. Walsh
Technical Publications (2)
Technical Information Files (5)